Biomaterials Advances 153 (2023) 213582

Contents lists available at ScienceDirect

Biomaterials Advances

journal homepage: www.journals.elsevier.com/materials-science-and-engineering-c

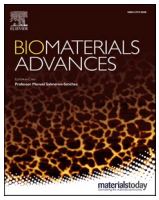

Electrospun fiber-based micro- and nano-system for delivery of high concentrated quercetin to cancer cells

Andrzej Hudecki [a,1], Iwona Rzeszutek [b,1], Anna Lewińska [b,1], Tymon Warski [a,c], Anna Baranowska-Korczyc [d], Renata Wojnarowska-Nowak [e], Gabriela Betlej [b], Anna Deręgowska [b], Jacek Hudecki [f], Dorota Łyko-Morawska [g], Wirginia Likus [h], Aleksandra Moskal [b], Piotr Krzemiński [e], Małgorzata Cieślak [d], Małgorzata Kęsik-Brodacka [i], Aleksandra Kolano-Burian [a,*], Maciej Wnuk [b,*]

[a] Lukasiewicz Research Network-Institute of Non-Ferrous Metals, Gliwice, Poland
[b] Institute of Biotechnology, University of Rzeszow, Rzeszow, Poland
[c] PhD School, Faculty of Mechanical Engineering, Silesian University of Technology, Gliwice, Poland
[d] Lukasiewicz Research Network - Lodz Institute of Technology, Lodz, Poland
[e] Center for Microelectronics and Nanotechnology, Institute of Materials Engineering, University of Rzeszow, Rzeszow, Poland
[f] Department of Laryngology, Faculty of Medical Sciences in Katowice, Medical University of Silesia, Katowice, Poland
[g] Department of General Surgery, Vascular Surgery, Angiology and Phlebology, Medical University of Silesia, Katowice, Poland
[h] Department of Anatomy, Faculty of Health Sciences in Katowice, Medical University of Silesia, Katowice, Poland
[i] National Medicines Institute, Warsaw, Poland

ARTICLE INFO

Keywords:
Electrospun fibers
Quercetin
Apoptosis
Osteosarcoma
Breast cancer
HSP

ABSTRACT

The anticancer potential of quercetin (Q), a plant-derived flavonoid, and underlining molecular mechanisms are widely documented in cellular models *in vitro*. However, biomedical applications of Q are limited due to its low bioavailability and hydrophilicity. In the present study, the electrospinning approach was used to obtain polylactide (PLA) and PLA and polyethylene oxide (PEO)-based micro- and nanofibers containing Q, namely PLA/Q and PLA/PEO/Q, respectively, in a form of non-woven fabrics. The structure and physico-chemical properties of Q-loaded fibers were characterized by scanning electron and atomic force microscopy (SEM and AFM), X-ray powder diffraction (XRD), differential scanning calorimetry (DSC), goniometry and FTIR and Raman spectroscopy. The anticancer action of PLA/Q and PLA/PEO/Q was revealed using two types of cancer and nine cell lines, namely osteosarcoma (MG-63, U-2 OS, SaOS-2 cells) and breast cancer (SK-BR-3, MCF-7, MDA-MB-231, MDA-MB-468, Hs 578T, and BT-20 cells). The anticancer activity of Q-loaded fibers was more pronounced than the action of free Q. PLA/Q and PLA/PEO/Q promoted cell cycle arrest, oxidative stress and apoptotic cell death that was not overcome by heat shock protein (HSP)-mediated adaptive response. PLA/Q and PLA/PEO/Q were biocompatible and safe, as judged by *in vitro* testing using normal fibroblasts. We postulate that PLA/Q and PLA/PEO/Q with Q releasing activity can be considered as a novel and more efficient micro- and nano-system to deliver Q and eliminate phenotypically different cancer cells.

1. Introduction

Drug-delivery systems (DDS) are very useful approaches in anticancer strategies to maximize the drug-mediated therapeutic effects in cancer cells and minimize adverse side effects in normal neighboring cells and tissues [1]. The mode of delivery can affect the pharmacokinetics, distribution, cellular uptake and metabolism, excretion and clearance, as well as toxicity of a drug [1]. Nanocarriers such as nanoparticles, nanofibers, nanogels, micelles, and microspheres can be used to deliver anticancer drugs, which otherwise in an unmodified form are too toxic, insoluble, rapidly cleared or unstable as free molecules for biological applications [1–3].

* Corresponding authors.
E-mail addresses: aleksandra.kolano-burian@imn.lukasiewicz.gov.pl (A. Kolano-Burian), mwnuk@ur.edu.pl (M. Wnuk).
[1] These authors contributed equally to this work.

https://doi.org/10.1016/j.bioadv.2023.213582
Received 17 April 2023; Received in revised form 28 July 2023; Accepted 6 August 2023
Available online 9 August 2023

Electrospinning, a fiber fabrication method, utilizes high voltage and polymers to produce fiber-based matrix with interconnected pores that can be loaded with a number of therapeutic agents [2–4]. Electrospun structures are characterized by large surface area, high porosity and tunable morphology and these features can be modulated to provide micro- and nanofibers with dedicated physicochemical properties, degradation kinetics, and drug release profiles [2–5]. A plethora of polymers is considered to obtain electrospun fiber-based drug delivery micro- and nano-systems, such as natural polymers, for example, hyaluronic acid, chitosan, dextran, gelatin, collagen, and synthetic polymers, for example, poly(lactic acid) (PLA), poly(lactic-co-glycolic acid) (PLGA), poly(ε-caprolactone) (PCL), and their combinations [2–6]. Furthermore, small molecule drugs, proteins and nucleic acids can be encapsulated within or immobilized onto the electrospun fibers for controlled drug release for biomedical applications in oncology and regenerative medicine [2–6].

Quercetin, a pentahydroxyflavone ubiquitously present in edible vegetables, fruits and wine, is characterized by beneficial bioactive effects, such as antioxidant, anticancer, antidiabetic, anti-inflammatory, antibacterial, antiarthritic, neuro- and cardioprotective, and wound healing properties [7–9]. Anticancer action of quercetin is documented in a number of cancer cell types that is based on the modulation of the activity of numerous signaling pathways, for example, PI3K/Akt and Ras/ERK, interactions with proteins, and induction of oxidative stress that may result in apoptotic cell death and the inhibition of cell proliferation, migration, invasion, and angiogenesis [7,8,10–13]. However, biomedical applications of quercetin may be limited due to its low oral bioavailability, because of poor aqueous solubility and permeability, instability in stomach and intestine, short biological half-life, and extensive first past metabolism in the liver before reaching the systemic circulation [7,8]. A number of approaches was designed and tested to improve the uptake and bioavailability of quercetin, for example, quercetin encapsulation in liposomes and fabrication of quercetin nanoparticles and nanocrystals [7,8]. Data on anticancer potential of quercetin-loaded electrospun nanofibers are scarce [14–16]. The authors limited their analysis to only one cancer cell line [14–16]. Thus, more comprehensive studies are needed to document if electrospun fiber-based micro- and nano-delivery of quercetin may potentiate its antineoplastic activity.

In the present study, electrospun fibers containing polylactide (PLA), polyethylene oxide (PEO) and high concentrated quercetin (9 %) were fabricated, and their effects were evaluated against nine cancer cell lines, namely osteosarcoma cells (MG-63, U-2 OS, SaOS-2 cell lines) and breast cancer cells (SK-BR-3, MCF-7, MDA-MB-231, MDA-MB-468, Hs 578T, and BT-20 cell lines) with different genetic traits and phenotypic features. Improved anticancer action of quercetin in a form of quercetin-loaded electrospun fibers was documented and discussed.

2. Materials and methods

2.1. Preparation of quercetin-loaded fibers and the analysis of quercetin loading efficiency

The synthetic polymeric materials polylactide (PLA, CAS No.: 26100-51-6) and polyethylene oxide (PEO, average Mv 100,000, CAS No.: 25322-68-3) (Merck KGaA, Darmstadt, Germany) were used to prepare quercetin (Q)-loaded fibers. Acetone (CAS No.: 67-64-1, ≥99.9 %) and chloroform (CAS No.: 67-66-3, ≥99.5 %) solution (70:30, Chemland, Stargard, Poland) was applied and PLA and PEO were used at a ratio of 10 to 1. Free quercetin (Q, CAS No: 849061-97-8, Q4951, Merck KGaA, Darmstadt, Germany, ≥95 % (HPLC)) was used at 9 %. To obtain the single-component (PLA), two-component (PLA/Q and PLA/PEO) and multi-component (PLA/PEO/Q) fibers, the electrospinning machine (TL-BM device, TONG LI TECH, Shenzhen, China) equipped with a working chamber, control panel, infusion pumps with adjustable flow rates of μl/min and ml/h, and standard electrospinning nozzles was used. During electrospinning, nanofibers and microfibers were applied to a rotary manifold for 1 h. After dissolution, the solutions were placed in dedicated tanks and, using a system of Teflon tubes, were transported to the working chamber for the conversion into micro- and nanofibers using an electrostatic field (PLA, PLA/Q, PLA/PEO and PLA/PEO/Q). The fibers falling on the surface of the collector formed then a non-woven fabric. The following conditions were applied: solution flow 20 ml/h, rotary collector, collector speed 20 rpm, voltage 0.95–1.00 kV/cm, solution temperature 25 °C, temperature in the working chamber 23 °C, relative humidity in the working chamber 35 %. Upon preparation of quercetin-loaded fibers using 9 % quercetin, quercetin loading efficiency was analyzed. To do so, fiber mats (1 cm diameter) were weighed and 1 ml of dichloromethane (DCM, CAS No.: 75-09-2, 34856, Merck KGaA, Darmstadt, Germany, ≥99.8 % (HPLC)) was added to dissolve fiber mats at room temperature for 2 h. Next, the amount of quercetin was analyzed in a solution of dimethyl sulfoxide (DMSO): Dulbecco's phosphate buffered saline (DPBS) (1:10) (DMSO, CAS No.: 67-68-5, grade: molecular biology, ≥99.5 % (GC)) using a UV spectrophotometer (the absorbance was measured at 365 nm). The absorbance of solutions upon PLA and PLA/PEO incubations were used as control (background) absorbance for PLA/Q and PLA/PEO/Q quercetin loading efficiency experiments, respectively. The concentration of quercetin (μg/ml) was read against the calibration curve. The incorporation efficiency of the fibers was calculated using the following formula:

$$\text{Incorporation efficiency (IE)}\ [\%] = (\text{the amount of quercetin loaded/theoretical quercetin amount in the fiber}) \times 100.$$

2.2. Physico-chemical characterization of quercetin-loaded fibers

2.2.1. Optical microscopy

The gross morphology of fibers was analyzed using Olympus DSX1000 digital microscope and dedicated software (OLYMPUS, Shinjuku Monolith, Shinjuku-ku, Tokyo, Japan).

2.2.2. Scanning electron microscopy (SEM)

The fiber structure was studied using a ZEISS SUPRA 25 scanning electron microscope (Jena, Germany) using an accelerating voltage of 3–25 kV. The samples were sputtered with gold and then placed in the working chamber of the SEM microscope, where analysis was carried out at magnifications of 5000–10,000×. The fiber diameter and its spatial distribution were investigated using Digital Micrograph 365 software.

2.2.3. Atomic force microscopy (AFM)

Atomic force microscopy (AFM) measurements were carried out using Innova instrument (Bruker Nano Inc., Santa Barbara, CA, USA) to investigate the morphology and roughness of quercetin-loaded fibers. AFM tapping mode was used to analyze the morphology of the fibers using silicon cantilevers (TESPA-V2 from Bruker Nano Inc.) with a spring constant of ~37 N/m, a resonance frequency of 331 kHz, and an apex radius of curvature ~7 nm. The measurements were performed at ambient air (22–24 °C). The AFM images and roughness data were analyzed using the NanoScope Analysis software.

2.2.4. BET surface area analysis

Brunauer-Emmett-Teller (BET) gas adsorption-based method was used to assess specific surface area and porosity using a Gemini VII 2390t specific surface area analyzer (Micrometrics, Ottawa, Canada). Samples (0.2 g) were subjected to drying under vacuum at 30 °C for 24 h to remove moisture and adsorbed gases. The dried samples were further placed in the device and the environment for the measurement was created (making a vacuum, immersing the sample in nitrogen, determining the measurement). For adsorption and desorption, pressures ranging from 0.1 to 1 mmHg were adopted. Nitrogen with a purity of 5.0 was used as a measurement gas.

2.2.5. X-ray diffraction analysis (XRD)

The phase structure of quercetin-loaded fibers was determined by wide-angle X-ray diffraction using a Rigaku MiniFlex 600 diffractometer (Rigaku, Tokyo, Japan) equipped with a copper CuKα radiation source ($\lambda = 0.1542$ nm), a Kβ Ni filter and an ultrafast silicon D/teX detector. The measurements were carried out at room temperature (22–24 °C), in the 2θ 3–90° angle range, with a measurement speed of 1.5°/min and a measurement step of 0.02°.

2.2.6. Weight loss analysis

In order to evaluate the initial weight loss of the polymeric materials, the following steps were included: samples were prepared from the obtained materials, each sample was weighed using an analytical balance, the samples were immersed in distilled water at 37 °C for 24, 48 and 72 h, the samples were removed then from the water, frozen at −40 °C for 24 h and freeze-dried then for 24 h using a freeze-dryer to evaporate the water. After drying, the samples were weighed again and the difference in the mass after 24, 48 and 72 h of water treatment was calculated.

2.2.7. Differential thermal analysis/thermogravimetry (DTA/TG)

Heat flow (DTA) and mass change (TG) measurements were performed using a simultaneous thermal analyzer STA Netzsch F3 Jupiter (Selb, Germany) in an argon atmosphere. The heating rate was 10 K/min in the range from room temperature (25 °C) to 600 °C. Tested samples weighed 13–20 mg. Aluminium oxide crucibles were used for the measurements. The temperatures and mass changes were read out using dedicated software.

2.2.8. Wettability

The contact angle of electrospun non-woven fabric was measured using a PGX Goniometer (Fibro Systems AB, Hägersten, Sweden) with a dynamic method. Distilled water was automatically applied at a constant volume of 4 ± 0.2 μl to the tested surface with the goniometer. At least eight measurements were considered for each sample. The following conditions were used: relative humidity 49 ± 2 %, temperature 22 ± 1 °C.

2.2.9. Fourier-transform infrared spectroscopy (FTIR)

FTIR absorption spectra were recorded using a BRUKER Vertex 70 FTIR spectrometer (Billerica, MA, USA) with an ATR Golden Gate diamond adapter, in the spectral range from 600 cm^{-1} to 4000 cm^{-1} with a resolution of 4 cm^{-1}.

2.2.10. Raman spectroscopy

The Raman spectra were obtained using an inVia Micro Raman Renishaw spectrometer combined with a Leica DM 2500 M microscope (Renishaw, Wotton-under-Edge, Gloucester-shire, England, UK). The measurements were taken with a backscattering geometry, with 785 nm laser as an excitation source, in three randomly selected positions. The exposure time was set at 10 s with triple scan accumulation. The data were collected in the spectral range of 200–4000 cm^{-1} with spectral resolution over 1 cm^{-1}. The measurements were carried out with a 50× magnification. Baseline correction and normalization were performed during data processing.

2.3. Cell lines and fiber treatment

The following human normal and cancer cell lines were used, namely normal foreskin fibroblasts (BJ cells, CRL-2522™, ATCC, Manassas, VA, USA), osteosarcoma cell lines MG-63 (86051601), U-2 OS (92022711) and SaOS-2 (89050205) (ECACC, Public Health England, Porton Down, Salisbury, UK) and breast cancer cells SK-BR-3 (HTB-30™), MCF-7 (HTB-22™), MDA-MB-231 (HTB-26™), MDA-MB-468 (HTB-132™), Hs 578T (HTB-126™), and BT-20 (HTB-19™) (ATCC, Manassas, VA, USA). Cells were grown at 37 °C in DMEM medium supplemented with 10 % (v/v) FBS and 100 U/ml penicillin, 0.1 mg/ml streptomycin, and 0.25 μg/ml amphotericin B (Corning, Tewksbury, MA, USA) in a controlled humidified atmosphere containing 5 % CO_2. In the case of BJ cells, proliferatively active fibroblasts were only considered (cells at population doubling levels between 30 and 40) [17]. Cells were treated with four types of electrospun fibers, namely polylactide-only fibers (denoted as PLA), polylactide/polyethylene oxide-only fibers (denoted as PLA/PEO), polylactide fibers containing quercetin (denoted as PLA/Q) and polylactide/polyethylene oxide fibers containing quercetin (denoted as PLA/PEO/Q) for 24 and 48 h. For cell culture in 6-well plates, Q-loaded fibers containing quercetin, in a form of non-woven fabrics, were used with the diameter of 2 cm and the mass of 3.4 and 5.5 mg for PLA/Q and PLA/PEO/Q, respectively. Taking into account that 2×10^5 cells were seeded, cells were stimulated with quercetin at 15.3 and 24.75 ng of quercetin per cell, for PLA/Q and PLA/PEO/Q, respectively.

For MTT test, a free quercetin at the concentrations of 12.5, 25 and 50 μM (Q, Merck KGaA, Darmstadt, Germany) was also used.

2.4. Quercetin release in cell-free in vitro system

PLA/Q and PLA/PEO/Q were left in deionized water for up to 72 h at 37 °C and the amount of released quercetin into an aqueous solution was then determined using UV/VIS spectroscopy based on the absorbance measurements at 365 nm. The absorbance of solutions upon PLA and PLA/PEO incubations were used as control (background) absorbance for PLA/Q and PLA/PEO/Q release experiments, respectively. The concentration of quercetin (μg/ml) was read against the calibration curve. The quercetin release is presented as ΔC (μg/ml).

2.5. Quercetin-loaded fiber uptake

To examine the cellular uptake of PLA/Q and PLA/PEO/Q, osteosarcoma and breast cancer cells were cultured in a 12-well plate at a cell density of 1×10^5 cells per well for 24 h. PLA, PLA/PEO, PLA/Q and PLA/PEO/Q were then added and cells were stimulated for 48 h. Quercetin uptake was analyzed using imaging flow cytometry (Amnis® FlowSight® imaging flow cytometer) and IDEAS software (version 6.2.187.0, Luminex Corporation, Austin, TX, USA). Two parameters were considered, namely Normalized Frequency and Intensity_MC_Ch03. Representative histograms are presented.

2.6. MTT assay

Quercetin-loaded fiber-mediated changes in the metabolic activity of normal and cancer cells were assessed using MTT test [18]. Briefly, cells were seeded onto a 96-well plate at a cell density of 5×10^3 cells per well and incubated at 37 °C for 24 h. Fibers (PLA, PLA/PEO, PLA/Q and PLA/PEO/Q) were added for 48 h and the metabolic activity was then measured as previously described [18]. The effects of 12.5, 25, and 50 μM quercetin were also studied. Metabolic activity at untreated conditions is considered as 100 %.

2.7. Wound healing assay

Quercetin- loaded fiber-mediated changes in cell migration was analyzed using *in vitro* scratch assay (wound healing assay) [19]. Osteosarcoma cells were seeded at a cell density of 2×10^5 in a 6-well plate and cultured at 37 °C for 24 h. The monolayer of cells was then wounded with a micropipette tip (10 μl) forming a scratch. The medium was then exchanged and fibers (PLA, PLA/PEO, PLA/Q and PLA/PEO/Q) were added for up to 48 h. Cell migration-based wound healing (the distance between two sides of a wound) was then documented and analyzed using the Olympus IX71 microscope and dedicated software.

2.8. Cell proliferation-related parameters

Quercetin-loaded fiber-mediated changes in osteosarcoma cell number, phases of cell cycle, and the levels of cell cycle inhibitor p21 were analyzed as biomarkers of cell proliferation upon 48 h stimulation with fibers. The cell count was calculated using TC10™ Automated Cell Counter (Bio-Rad, Hercules, CA, USA). DNA content-based analysis of the phases of the cell cycle (G0/G1, S and G2/M) was conducted using a Muse® Cell Analyzer and a Muse® Cell Cycle Assay Kit according to the manufacturer's instructions (Luminex Corporation, Austin, TX, USA). Representative histograms (%) are presented. The nuclear levels of p21 were revealed using immunostaining with dedicated primary antibody anti-p21 (1:800, MA5–14949) and secondary antibody conjugated to Texas Red (1:1000, T2767) (Thermo Fisher Scientific, Waltham, MA, USA). Digital cell images were captured using a confocal imaging system IN Cell Analyzer 6500 HS (Cytiva, Marlborough, MA, USA). Quantitative analysis of p21 levels in the nucleus was conducted using IN Carta software (Cytiva, Marlborough, MA, USA). Nuclear levels of p21 are presented in relative fluorescence units (RFU).

2.9. Apoptotic cell death

Quercetin-loaded fiber-induced apoptosis in osteosarcoma and breast cancer cells was studied using Muse® Cell Analyzer and Muse® Annexin V and Dead Cell Assay Kit (Luminex Corporation, Austin, TX, USA) [18]. Briefly, after 48 h stimulation with the fibers, four subpopulations (%) were distinguished, namely live (Annexin V-negative, 7-AAD-negative), early apoptotic (Annexin V-positive, 7-AAD-negative), late apoptotic (Annexin V-positive, 7-AAD-positive) and necrotic cells (Annexin V-negative, 7-AAD-positive). Representative dot-plots (%) are presented.

2.10. Oxidative stress

Quercetin-loaded fiber-induced oxidative stress was studied using Muse® Cell Analyzer and Muse® Oxidative Stress Kit (Luminex Corporation, Austin, TX, USA) containing a superoxide indicator, a fluorogenic probe dihydroethidium [18]. After 48 h stimulation with the fibers, two subpopulations were analyzed, namely superoxide-positive and superoxide-negative cells. Representative histograms (%) are presented.

2.11. Phosphorylation status of Akt and ERK1/2

Quercetin-loaded fiber-mediated changes in the activity of extracellular signal-regulated kinase 1/2 (ERK1/2) and Akt (protein kinase B) were analyzed using Muse® Cell Analyzer and Muse®PI3K/MAPK Dual Pathway Activation Kit using two conjugated antibodies, anti-phospho Akt (Ser473)-Alexa Fluor™ 555 and anti-phospho ERK1/2 (Thr202/Tyr204, Thr185/Tyr187)-PECy5 (Luminex Corporation, Austin, TX, USA) according to the manufacturer's instructions. Briefly, after 48 h stimulation with the fibers, four subpopulations were revealed (%), namely pERK1/2-negative and pAkt-negative (no activation), pERK1/2-positive and pAkt-negative (ERK1/2 activation), pERK1/2-positive and pAkt-positive (ERK1/2 and Akt dual activation), pERK1/2-negative and pAkt-positive (Akt activation). Representative dot-plots (%) are presented.

2.12. HSP70 and HSP90 levels

After treatments with PLA, PLA/PEO, PLA/Q and PLA/PEO/Q, cells were fixed and immunostained as described elsewhere [18]. Briefly, cells were incubated with the primary antibodies anti-HSP70 (1:200, PA5-14521) and anti-HSP90 (1:200, MA1-10373) (Thermo Fisher Scientific, Waltham, MA, USA) at 4 °C overnight. Dedicated fluorochrome conjugated secondary anti-mouse and anti-rabbit antibodies (1:1000, T2767, A10524) (Thermo Fisher Scientific, Waltham, MA, USA) were then used for 1 h incubation at room temperature. The nuclei were detected using Hoechst 33342 staining. Digital cell images were acquired using a confocal imaging system IN Cell Analyzer 6500 HS (Cytiva, Marlborough, MA, USA) or Amnis® FlowSight® imaging flow cytometer (Luminex Corporation, Austin, TX, USA). Quantitative analysis was performed using IN Carta software (Cytiva, Marlborough, MA, USA) and IDEAS software version 6.2.187.0 (Luminex Corporation, Austin, TX, USA), respectively. HSP70 and HSP90 levels (total, nuclear and cytosolic) are presented as relative fluorescence units (RFU).

2.13. Cellular thermal shift assay (CETSA)

The interactions between quercetin and HSP70 were analyzed using cellular thermal shift assay (CETSA) with minor modifications [20]. Briefly, 1.2×10^7 Hs 578T breast cancer cells were treated with 50 μM quercetin for 24 h. As a vehicle, dimethyl sulfoxide (DMSO, CAS No.: 67-68-5, grade: molecular biology, ≥99.5 % (GC)) was used. Cells were then collected and resuspended in DPBS (Dulbecco's phosphate buffered saline) containing a protease inhibitor cocktail (Roche, Basel, Switzerland). Cell suspensions (100 μl) were heated to dedicated temperatures for 3 min using a thermal cycler, followed by 3 min cooling at room temperature. Cells were then incubated at −80 °C overnight, and subjected to two freeze-thaw cycles. For each cycle, samples were incubated at −80 °C for 30 min, placed at room temperature for 5 min, and vortexed vigorously. Lysates were then centrifuged (14,000 rpm, at 4 °C for 20 min). The supernatants were further processed for western blotting protocol [18]. The primary anti-HSP70 (1:1000, PA5-34772) and secondary HRP-linked antibody (1:3000, 7074) (Thermo Fisher Scientific, Waltham, MA, USA, Cell Signaling Technology, Danvers, MA, USA) were used. Densitometric measurements were performed and data were normalized to DMSO-treated sample at 50.4 °C.

2.14. Hemocompatibility test

The biocompatibility of quercetin-loaded fibers was studied using *in vitro* hemolysis test [21]. Briefly, 100 μl of whole blood samples were incubated with PLA, PLA/PEO, PLA/Q and PLA/PEO/Q at 37 °C for 24 and 48 h. The absorbance was then measured in the supernatants at 541 nm using a Tecan Infinite®M200 absorbance mode microplate reader (Tecan Group Ltd., Männedorf, Switzerland). The treatment with 37.5 mM KCl served as a positive control (CTR). Hemolytic activity of CTR was considered as 100 %.

2.15. Statistical analysis

The data were calculated as the mean ± SD of at least three independent experiments. Box and whisker plots with median, lowest, and highest values were also considered. Fiber-treated and non-treated groups were compared using one-way analysis of variance (ANOVA) followed by Dunnett's multiple comparison test. Probability values (p) of <0.05 were assumed as statistically significant. Statistical analysis was performed using the GraphPad Prism 8 software.

3. Results and discussion

In the present study, polylactide (PLA) and/or PLA and polyethylene oxide (PEO) were applied to obtain quercetin (Q)-loaded fibers (PLA/Q and PLA/PEO/Q, respectively) for biomedical applications. Q-loaded fibers were prepared using 9 % quercetin and electrospinning approach. Upon preparation of Q-loaded fibers, quercetin loading efficiency was analyzed using UV/VIS spectroscopy and dichloromethane as a solvent. Incorporation efficiency (IE) was established to be 84 ± 2 % and 91 ± 2 % for PLA/Q and PLA/PEO/Q, respectively.

3.1. The structure and physico-chemical properties of quercetin-loaded fibers

The optical microscopy-based analysis of gross morphology of PLA, PLA containing quercetin (PLA/Q), PLA/PEO, and PLA and PEO containing quercetin (PLA/PEO/Q) fibers is shown in Fig. S1 (top). The fiber diameter was determined after conducting twenty measurements at randomly selected areas (Fig. S1, bottom). The average fiber diameter values were similar among four fiber categories (about 3 μm, Fig. S1, bottom). However, different fiber diameter ranges were observed (Fig. S1, bottom). The diameter distribution of PLA, PLA/Q, PLA/PEO and PLA/PEO/Q fibers was then further evaluated using scanning electron microscopy (Figs. S2A–C, S3A–C, S4A–C and Fig. 1A–C). PLA non-woven fabric contained 18 % of nanofibers (diameter below 1000 nm) and 82 % microfibers (diameter above 1000 nm) (Fig. S2C). Addition of 9 % quercetin to PLA fibers resulted in a decrease of nanofiber fraction (4 %) compared to PLA fibers (Fig. S3C). The presence of PEO in PLA fibers (PLA/PEO) dramatically affected the fiber diameter (Fig. S4C). Only PLA/PEO microfibers with diameter above 2.01 μm were observed (100 %) (Fig. S4C). When quercetin was added to PLA/PEO fibers, a fraction of PLA/PEO/Q nanofibers appeared (42 %) (Fig. 1C). Thus, one can conclude that the presence of quercetin significantly modulated the properties of obtained material, which, when subjected to an electrostatic field, was stretched much more intensely than this without the additive resulting in a significant reduction in diameter and the occurrence of two fractions (micro- and nanofibers) of almost equal proportion (58 and 42 %, respectively, Fig. 1C). Atomic force microscopy was also used to analyze the topography of fibers, but their surface roughness was the most important information they provided (Fig. S5). The level of roughness affects some fiber properties like biocompatibility, through conductive to cell adhesion, growth, and proliferation. The surface roughness should be considered especially in the design of the nanomaterials and nanocomposites for biomedical applications. The fiber diameter was between 2 and 3 μm, which is consistent with the results obtained using other microscopic methods. The surface roughness analysis was performed on the topography AFM data (Fig. S5E). The values for four roughness parameters for PLA, PLA/Q, PLA/PEO and PLA/PEO/Q surfaces are presented in Fig. S5E. The highest roughness was observed in the case of PLA/PEO (29 nm), whereas the roughness of other surfaces was comparable based on roughness average (Ra) values (between 10 and 14 nm, Fig. S5E). The specific surface area (m^2/g) was also evaluated using BET method (Fig. 1D). The specific surface area was associated with fiber diameter as the lowest specific surface area of 1.9 m^2/g was observed for PLA/PEO fibers with exclusive fraction of microfibers with diameter higher than 2.01 μm (Fig. 1D). Quercetin addition resulted in elevation of the specific surface area that was more pronounced in the case of PLA/PEO/Q compared to PLA/PEO than in case of PLA/Q compared to PLA (Fig. 1D). The fiber diameter may modulate the specific surface area of tested samples as well as the cellular response [22]. In turn, the specific surface area may affect the rate of release of bioactive substances/drugs [23]. The method of manufacture, morphology and drug concentration may determine the drug release profile. For example, microfluidic-electrospinning technique was used to obtain implantable trilayer structured fiber device (PLA- and poly(ε-caprolactone)-based platform) for time-programmed release of drug combination (a chemotherapy agent doxorubicin and an angiogenesis inhibitor apatinib) for synergistic treatment of breast cancer [24].

The analysis of XRD diffractograms revealed the existence of an amorphous structure in all fibers both Q containing and Q-free fibers (Figs. 1E, S2D, S3D and S4D, XRD diffractogram of free quercetin is also shown in Fig. S6A for comparison) that is important in terms of the bioavailability of drug-loaded polymeric material. The geometric properties of the fibers provoked the changes in the surface properties of the structures obtained and these consequently altered the dissolution rate of the materials, when exposed to an aqueous environment for 24, 48 and 72 h (Fig. 1F). A weight loss was considered as a parameter of dissolution process in water (Fig. 1F). PLA fibers were characterized by the weaker ability to dissolve in water (a weight loss of 1.57 % after 72 h incubation in water, Fig. 1F). The effect of quercetin in the case of PLA/Q fibers was only very slight compared to a weight loss of PLA after 72 h incubation in water (Fig. 1F). The highest weight loss of fibers in an aqueous environment was observed for PLA/PEO fibers with a weight loss of 8.69 % after 72 h incubation in water that is related to the leaching of PEO from the fiber material (Fig. 1F). This effect is not noticed in the case of PLA/PEO fibers containing quercetin (PLA/PEO/Q) (Fig. 1F). Thus, one can conclude that the presence of quercetin significantly limited the solubility of the polymer PEO (Fig. 1F). The thermogravimetric (TG) analysis was then performed in the relation to the change in the sample weight with heating (Figs. 1G, S2E, S3E and S4E, the thermogravimetric analysis of free quercetin is also shown in Fig. S6B for comparison). The addition of PEO and quercetin attenuated weight loss at 350 °C (Figs. 1G, S2E, S3E and S4E). For example, for PLA fibers at 350 °C, there was an almost 100 % loss of initial sample weight (Fig. S2E). At the same temperature for PLA/Q fibers, there was 95 % of weight loss (Fig. S3E). Thus, quercetin limited a weight loss. In the case of PLA/PEO fibers, 100 % sample weight loss occurred above 400 °C that is of course related to the addition of PEO to the PLA matrix (Fig. S4E). Again, the presence of quercetin in the PLA/PEO/Q fibers caused 95 % of weight loss at 400 °C (Fig. 1G). Thus, quercetin modulated the thermal stability of both PLA and PLA/PEO fibers.

All types of fibers were hydrophobic, as judged by water contact angle analysis (Figs. 1H, I, S2F, S3F and S4F). The highest hydrophobicity was shown for PLA non-woven fabric (the contact angle of 135 ± 4°) and the lowest was documented for PLA/PEO/Q non-woven fabric (the contact angle of 129 ± 3°) (Fig. 1I). The combination of PLA with PEO slightly affected the hydrophobicity of the samples tested, but this effect was insignificant (Fig. 1I).

Lastly, the chemical characterization of PLA, PLA/Q, PLA/PEO and PLA/PEO/Q fibers was provided using FTIR and Raman spectroscopy (Fig. 1J–M and Table S1). Infrared spectra showed that, in contrast to quercetin-free fibers, in the region of 1700 to 1500 cm^{-1}, there were four bands in the spectra of unattached quercetin and quercetin-loaded fibers (denoted as asterisks, Fig. 1J). The band of free quercetin recorded at 1663 cm^{-1} corresponded to stretching vibrations of the carbonyl group of C═O [25]. The band maximum of quercetin-loaded fibers shifted to lower frequencies of 1656 cm^{-1} due to the formation of hydrogen bonds with the polymer matrix using the ketone groups of quercetin [26] (Fig. 1K and L and Table S1). Characteristic bands for quercetin at 1607, 1560 and 1520 cm^{-1} were also observed in fibers containing quercetin and indicated C═C aromatic bond stretching [25] (Fig. 1K and L and Table S1). Incubation in water for 24, 48 and 72 h did not affect FTIR spectra of PLA/Q and PLA/PEO/Q (Fig. 1K and L). The vibrational spectroscopic characterization of PLA, PLA/Q, PLA/PEO and PLA/PEO/Q fibers was also performed using Raman spectroscopy (Fig. 1M). Raman spectra also varied between quercetin-free fibers (PLA and PLA/PEO) and fibers containing quercetin (PLA/Q and PLA/PEO/Q) that was manifested by the appearance or disappearance of certain spectral lines (Fig. 1M). Furthermore, we have decided to analyze more comprehensively the stability of Q-loaded fibers in aqueous solution over time using SEM (Table S2) and Raman spectroscopy (Fig. S7). First,

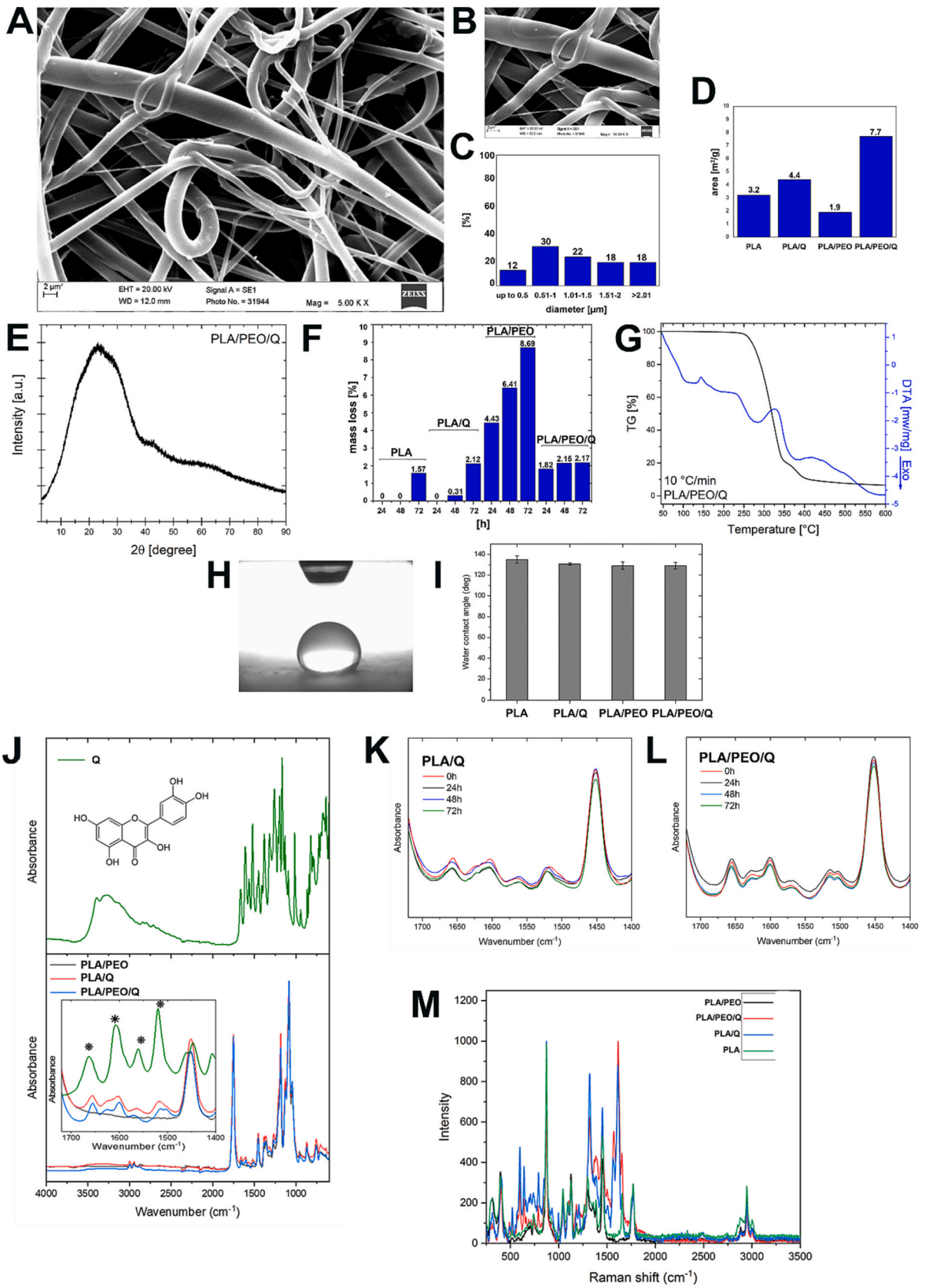

(caption on next page)

Fig. 1. Physico-chemical characterization of polylactide (PLA)-based fibers (PLA), PLA-based fibers containing quercetin (PLA/Q), PLA and polyethylene oxide (PEO)-based fibers (PLA/PEO) and PLA and PEO-based fibers containing quercetin (PLA/PEO/Q). Scanning electron microscopy (SEM) was used to analyze the geometry (A, B) and diameter distribution (C) of PLA/PEO/Q in acetone and chloroform solution; magnification 5000 (A), magnification 10,000 (B). (D) BET calculated specific surface area [m^2/g] for PLA, PLA/Q, PLA/PEO and PLA/PEO/Q. (E) XRD diffractogram of PLA/PEO/Q. (F) Weight loss [%]. Incubation in water for 24, 48 and 72 h was considered. (G) Differential thermal analysis/thermogravimetry (DTA/TG) measurements to analyze heat flow (DTA) and mass change (TG) during heating of PLA/PEO/Q. (H) The analysis of the contact angle of PLA/PEO/Q using PGX goniometer. (I) wettability angle test results for PLA, PLA/Q, PLA/PEO and PLA/PEO/Q. (J) FTIR spectra of PLA/PEO, PLA/Q and PLA/PEO/Q (bottom). FTIR spectrum of free quercetin (Q) along with the chemical formula for quercetin is shown for comparison (top). Asterisks were used to indicate four bands in the spectra of free quercetin and quercetin-loaded fibers in the region of 1700 to 1500 cm^{-1} (in a frame, bottom). FTIR spectra of PLA/Q (K) and PLA/PEO/Q (L) recorded immediately after formation in a solution of acetone and chloroform on a flat collector surface (0 h) and after 24, 48 and 72 h incubation in water (24, 48 and 72 h, respectively). (M) Raman spectra of PLA, PLA/Q, PLA/PEO and PLA/PEO/Q.

SEM-based analysis of fiber diameter over time was performed (Table S2). For PLA samples, the effect of the incubation in distilled water was evident. A decrease in fiber diameter was observed as evidenced by an increase in the presence of fibers below 2 μm from 68 % for PLA (at 0 h) to 87 % for PLA (at 96 h), the decrease in fiber diameter may indicate a gradual degradation process of PLA. For PLA/Q samples, the addition of quercetin to PLA slightly altered the diameter of the resulting PLA/Q (at 0 h) fibers compared to the initial quercetin-free PLA (at 0 h) polylactide samples. For PLA/PEO samples, when comparing the PLA (at 0 h) sample with PLA/PEO (at 0 h), the effect of the PEO polymer on the fiber diameter is noticeable, thus producing PLA/PEO fibers with a significantly larger diameter than PLA. Upon incubation in water, PEO dissolves in the test samples, leading to a decrease in fiber diameter over time. The study showed that after 96 h of sample incubation in water, the fraction of fibers with diameters below 2 μm increased in PLA/PEO samples from 0 % for PLA/PEO (at 0 h) to 74 % for PLA/PEO (at 96 h). This huge increase in the fiber fraction below 2 μm may explain why the weight loss of the PLA/PEO samples is the most pronounced compared to other samples (Fig. 1F). For PLA/PEO/Q samples as is the case for PLA/Q samples, the addition of quercetin significantly altered fiber diameter below 2 μm in the samples tested, a significant increase in fibers below 2 μm is observed from 0 % for PLA/PEO (at 0 h) to 82 % for PLA/PEO/Q (at 0 h). When immersed in water, a significant increase in fiber diameter (above 2 μm) is noticed, from 18 % for PLA/PEO/Q (at 0 h) to 100 % for PLA/PEO/Q (at 48 h) and 93 % for PLA/PEO/Q (at 96 h). This result is opposite compared to PLA/PEO samples, where a decrease in fiber diameter is observed over time. However, for the PLA/PEO/Q samples, the observed changes in the diameter of the samples may be related to the swelling of the PLA/PEO/Q fibers due to the absorption of water by the hydrophilic polymer PEO, whose dissolution and permeation into the aqueous solution may be hindered by the presence of quercetin, which is poorly soluble in water. The results of the study can be related to those shown in Fig. 1F, where, for the PLA/PEO sample, a significant loss of initial sample mass over time is observed, while for the PLA/PEO/Q sample, the loss of sample mass is less evident. Time-dependent changes in fiber composition were also studied upon incubation in aqueous solution for up to 96 h using Raman spectroscopy (Fig. S7). No differences were observed in the spectra of PLA samples before and after wetting in water (Fig. S7). The significant changes are visible after a longer incubation time (48 h and 96 h) in water (Fig. S7). This indicates a change in the chemical structure of the fibers, which may be associated with the degradation of the material. The disappearance of some bands has been recorded: band associated with CH_3 vibrations (2998 cm^{-1}, 1387 cm^{-1}, 1298 cm^{-1}, 1129 cm^{-1}), C-CH_3 vibrations (1045 cm^{-1}, 310 cm^{-1}), C═O (1769 cm^{-1}), C-CO (874 cm^{-1}). The appearance of new bands was also observed: 2949 cm^{-1}, 2907 cm^{-1} and 1320 cm^{-1} indicating a change in the structure of the environment of C—H bonds, intense band at 2245 cm^{-1} associated with the appearance of triple bonds or X = Y=C bonds, 1096 cm^{-1} characteristic for C-O-C and C—O in alcohols, 800 cm^{-1}, 516 cm^{-1} and 448 cm^{-1}, which are difficult to be clearly identified. No differences were observed in the spectra of PLA/Q samples before and after wetting in water (Fig. S7). No significant differences were observed in the spectra recorded for samples after incubation in water for 48 h and 96 h (Fig. S7). There is a general weakening of the intensity of the bands, but there is no change in the structure of the bands. This indicates fiber stability and no modification in the chemical structure of the material. No differences were observed in the spectra of PLA/PEO samples at different time points (Fig. S7). This indicates a good stability of the material, and no visible changes in the chemical structure. For PLA/PEO/Q samples, the noticeable changes are visible after 48 h and 96 h incubation time in water (Fig. S7). Some bands in the spectrum of the PLA/PEO/Q sample after a longer incubation time disappear or is weakened. The lines are related to the vibrations of chemical bonds in polymers (2948 cm^{-1}, 1771 cm^{-1}, 1452 cm^{-1}, 1390 cm^{-1}, 1044 cm^{-1}, 873 cm^{-1}, 404 cm^{-1}) as well as quercetin (1656 cm^{-1}, 1615 cm^{-1}, 1569 cm^{-1}, 789 cm^{-1}, 697 cm^{-1}). Some bands characteristic for polymers (1129 cm^{-1}, 1090 cm^{-1}) and quercetin (1319 cm^{-1}, 596 cm^{-1}) are still present. The changes in chemical structure of the material during incubation are also evidenced by the appearance of new chemical bonds manifested in additional spectral bands: 1549 cm^{-1}, 1479 cm^{-1}, 1414 cm^{-1}, 816 cm^{-1}, 542 cm^{-1}, 428 cm^{-1}.

3.2. The anticancer activity of quercetin-loaded fibers against osteosarcoma cells

Quercetin, a plant-derived flavonoid, has a plethora of biological activities including broad-spectrum anticancer properties; however, its biomedical applications are limited due to low bioavailability in biological systems [7–9,27]. To overcome these difficulties, a number of drug delivery nano-systems have been proposed [7,27,28]. In the present study, electrospun PLA and PLA/PEO fibers (Figs. 1, S1–5) were used as a micro- and nanoformulation to provide high concentrated quercetin into cancer cells of two different types, namely osteosarcoma and breast cancer cells and test their anticancer potential *in vitro*. Three OS cells were selected on the basis of differences in the activity of proliferation-related and cell death signaling pathways, DNA damage responses, and the maintenance of redox homeostasis [29]. Six breast cancer cells with different receptor status (ER-positive, triple negative, and HER2-positive) and mutation patterns were also considered [30,31]. Such approach allowed for the evaluation of broad-spectrum anticancer activity of quercetin-loaded fibers.

First, quercetin release in cell-free system *in vitro* was analyzed (Figs. 2A, S8A). PLA and PLA/PEO fibers containing quercetin were incubated in distilled water for up to 72 h. As one can observe in Fig. 2A, quercetin was released from Q-loaded fibers (*i.e.*, PLA/PEO/Q) at the concentrations between 4 μg/ml (24 h incubation of PLA/PEO/Q in aqueous solution) and 7.5 μg/ml (72 h incubation of PLA/PEO/Q in aqueous solution). In contrast to PLA/PEO/Q, the quercetin release from PLA/Q did not exceed 4 μg/ml (Fig. 2A). However, quercetin was released faster from PLA/Q than from PLA/PEO/Q (Fig. 2A). Quercetin-loaded fibers were also efficiently taken up by OS cells (MG-63 > SaOS-2 > U-2 OS) (Fig. 2B). The anticancer activity of quercetin-loaded fibers against OS cells was initially assessed using MTT assay (Fig. 2C). Three concentrations of free quercetin (12.5, 25 and 50 μM that corresponded to 3.75, 7.5 and 15 μg/ml) were used for comparative analysis (Fig. 2C). Except U-2 OS cells, free quercetin was not active against OS cells and normal BJ cells (Fig. 2C). In contrast, PLA/PEO/Q treatment resulted in almost 50 % decrease of metabolic activity of SaOS-2 cells ($p < 0.001$, Fig. 2C). The effects of quercetin-loaded fibers against normal BJ cells

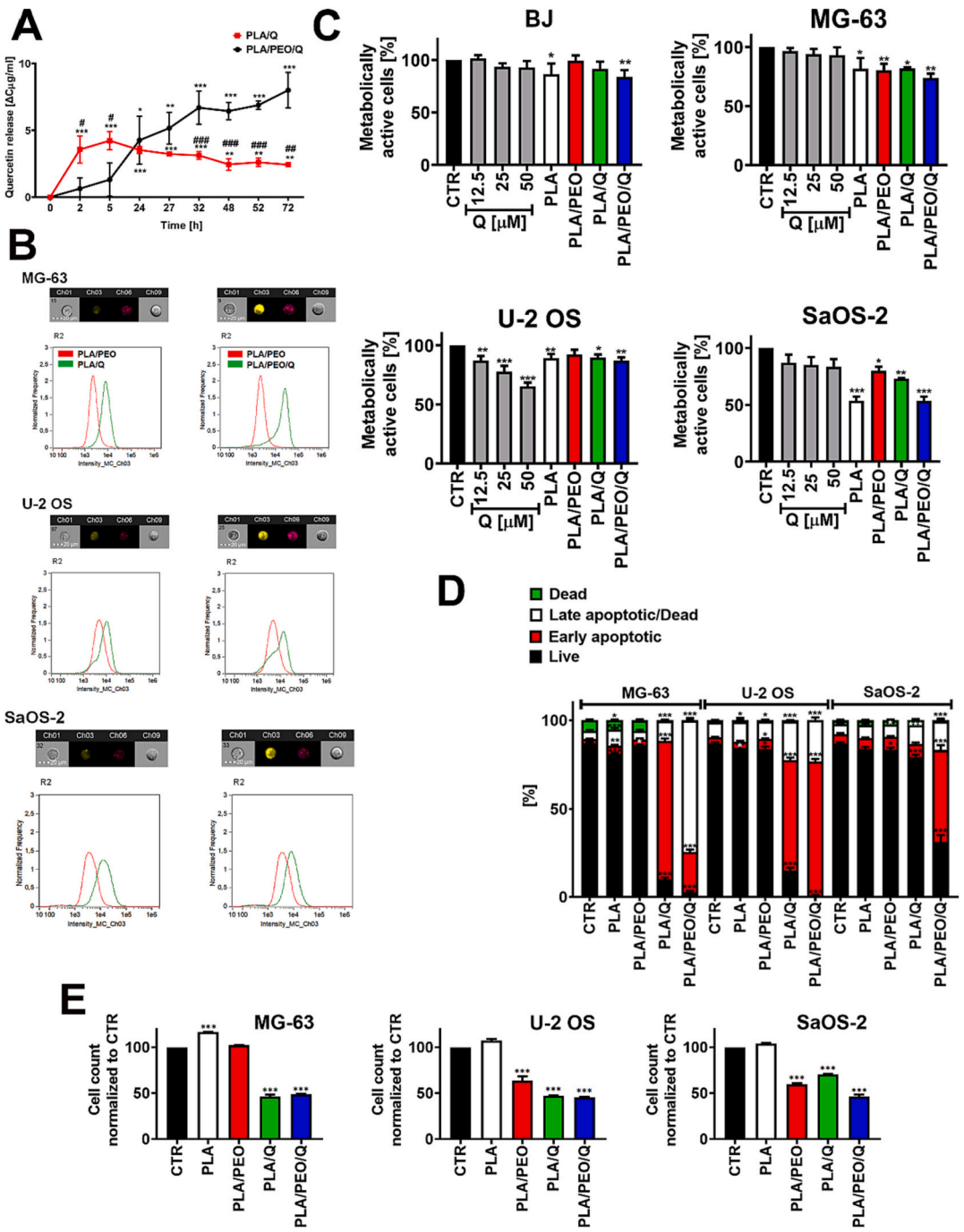

Fig. 2. PLA/Q and PLA/PEO/Q release (A), uptake (B) and mediated effects on metabolic activity (C), apoptosis induction (D) and cell number (E) in three osteosarcoma cell lines, namely MG-63, U-2 OS, and SaOS-2 cells. (A) The concentration of released quercetin into an aqueous solution was monitored using UV/VIS spectroscopy between 2 and 72 h incubation in cell-free *in vitro* system. The concentration of quercetin (μg/ml) was calculated using the calibration curve (Fig. S8A). The quercetin release is presented as ΔC (μg/ml). Bars indicate SD, $n = 3$, $^{***}p < 0.001$, $^{**}p < 0.01$, $^{*}p < 0.05$ compared to quercetin release at time 0 (ANOVA and Dunnett's *a posteriori* test), $^{###}p < 0.001$, $^{##}p < 0.01$, $^{#}p < 0.05$ compared to quercetin release from PLA/PEO/Q at appropriate time point (Student's *t*-test). Cells were treated with the fibers for 48 h (B–D). (B) Quercetin uptake was documented using imaging flow cytometry and dedicated software. Two parameters were applied, namely Normalized Frequency and Intensity_MC_Ch03. Representative microphotographs and histograms are presented. Ch01 and Ch09, bright field (BF); Ch03, Cyanine-3 (CY3)/orange; Ch06, side scatter (SSC). (C) Metabolic activity was analyzed using MTT test. Metabolic activity at untreated conditions is considered as 100 %. BJ human fibroblasts were used to also assess the effects of Q-loaded fibers on normal cells. (D) Apoptosis was evaluated using flow cytometry and dual staining approach, namely Annexin V and 7-AAD staining. Four subpopulations were distinguished, namely live cells (dual staining-negative), early apoptotic cells (Annexin V-positive), late apoptotic cells (dual staining-positive) and necrotic cells (7-AAD-positive). (E) Cell number was assessed using an automated cell counter. Data were normalized to control conditions. Bars indicate SD, n = 3, $^{***}p < 0.001$, $^{**}p < 0.01$, $^{*}p < 0.05$ compared to CTR untreated control (ANOVA and Dunnett's *a posteriori* test). CTR, control conditions; Q, treatment with a free quercetin; PLA, treatment with polylactide-based fibers; PLA/Q, treatment with polylactide-based fibers containing quercetin; PLA/PEO, treatment with polylactide and polyethylene oxide-based fibers; PLA/PEO/Q, treatment with polylactide and polyethylene oxide-based fibers containing quercetin.

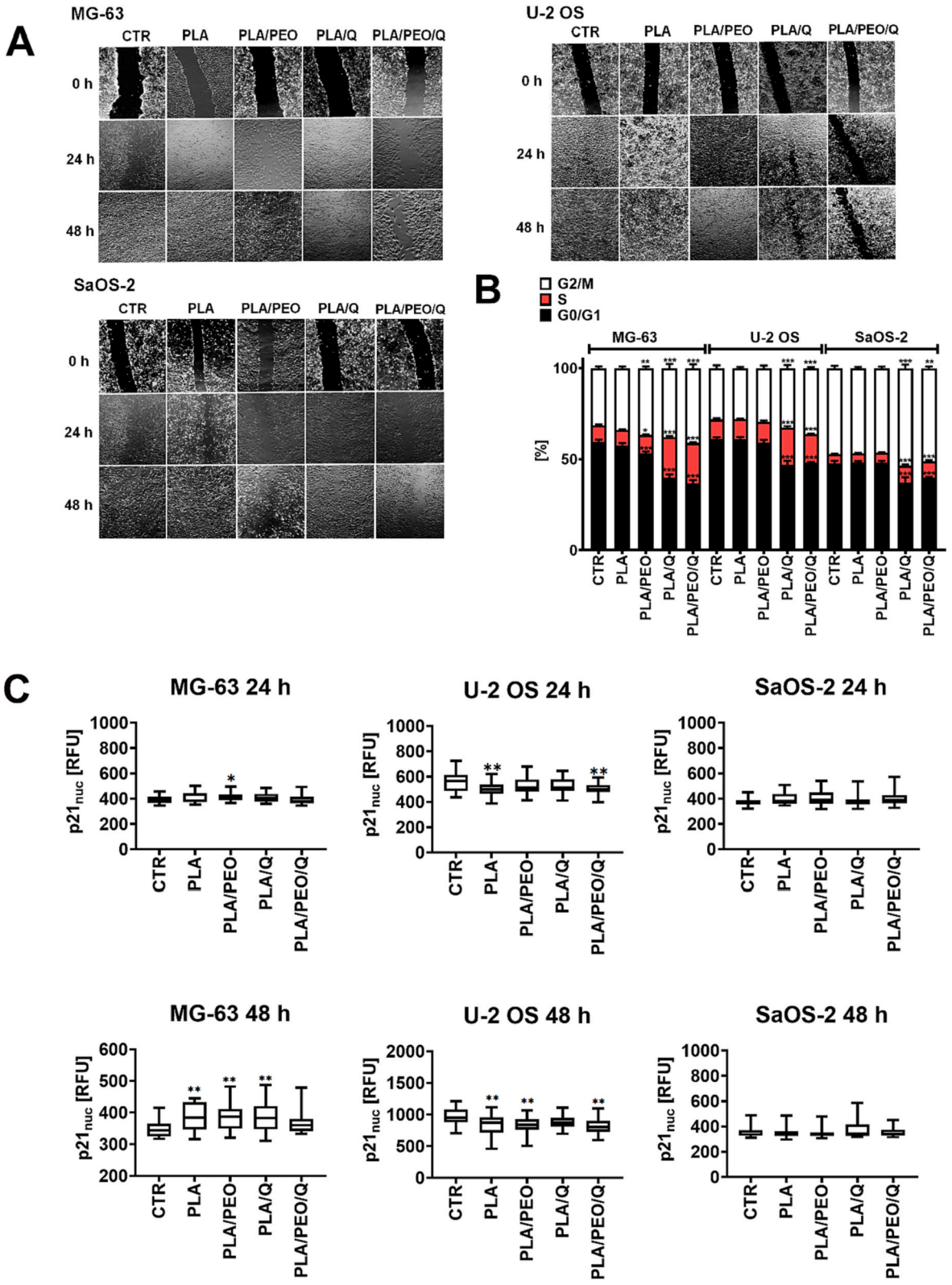

Fig. 3. Quercetin-loaded fiber-mediated effects on cell migration (A), cell cycle progression (B) and the levels of cell cycle inhibitor p21 (C) in three osteosarcoma cell lines, namely MG-63, U-2 OS and SaOS-2 cells. (A) Cell migration was evaluated using wound healing assay. Representative microphotographs are shown. (B) Cells were treated with the fibers for 48 h. The phases of the cell cycle were studied using DNA content-based analysis of cell cycle using flow cytometry and dedicated DNA staining. (C) Nuclear signals of p21 were revealed using imaging cytometry and dedicated anti-p21 antibody. Nuclear levels of p21 are shown as relative fluorescence units (RFU). Bars indicate SD or box and whisker plots are shown, n = 3, $^{***}p < 0.001$, $^{**}p < 0.01$, $^{*}p < 0.05$ compared to CTR untreated control (ANOVA and Dunnett's *a posteriori* test). CTR, control conditions; PLA, treatment with polylactide-based fibers; PLA/Q, treatment with polylactide-based fibers containing quercetin; PLA/PEO, treatment with polylactide and polyethylene oxide-based fibers; PLA/PEO/Q, treatment with polylactide and polyethylene oxide-based fibers containing quercetin.

were limited (Fig. 2C). We asked then if quercetin-based fiber-mediated changes in metabolic activity of OS cells (Fig. 2C) may reflect its cytotoxic (apoptosis induction, Figs. 2D and S8B) or cytostatic activity (a decrease in cell number, Fig. 2E). PLA/PEO/Q promoted a massive induction of apoptotic cell death in three OS cell lines (U-2 OS>MG-63 > SaOS-2) ($p < 0.001$, Fig. 2D). PLA/Q also induced apoptosis in MG-63 and U-2 OS cells ($p < 0.001$, Fig. 2D). Quercetin-loaded fiber-associated apoptosis was also accompanied by a decrease in cell number of about 50 % compared to control conditions in three OS cell lines ($p < 0.001$, Fig. 2E). Cytostatic activity of quercetin-based nanoplatforms was further evaluated in OS cells (Fig. 3). PLA/PEO/Q inhibited cell migration as judged by wound healing assay in three OS cell lines (Fig. 3A). PLA/Q and PLA/PEO/Q caused S and G2/M cell cycle arrest in three OS cell lines (Figs. 3B and S8C). Cytotoxic and cytostatic activity of quercetin in cellular models of osteosarcoma was studied in almost all cases at the concentrations ranging from 10 to 1000 μM and up to 48 h treatment [11]. The authors reported both quercetin-mediated G1/S and G2/M cell cycle arrest that was dependent on osteosarcoma cell line [11]. For example, quercetin (50 μM, 48 h stimulation) affected the G2/M phase of cell cycle of U-2 OS cisplatin (CDDP)-resistant cells that surprisingly was accompanied by decreased expression of cyclin D1, but not a diminution in cyclin B1 levels [32]. The authors concluded that quercetin-mediated changes in the G2/M phase of cell cycle may be executed by other cyclin B1-independent mechanisms [32]. In contrast, quercetin-mediated G2/M cell cycle arrest was accompanied by a decrease in cyclin B1 levels and cyclin B1-associated Cdc2 kinase activity and an increase in Cdk-inhibitor $p21^{CIP1/WAF1}$ levels in MCF-7 breast cancer cells [33]. Quercetin-induced apoptosis in MCF-7 cells was also attenuated by the expression of antisense-$p21^{CIP1/WAF1}$ [33]. Cytostatic activity of PLA/Q and PLA/PEO/Q was not mediated by elevated levels of p21 in OS cells (Fig. 3C). Perhaps other cell cycle inhibitors are involved in PLA/Q and PLA/PEO/Q-associated inhibition of cell proliferation in OS cells. This issue requires further elucidation.

As quercetin-based anticancer action may be mediated by oxidative stress and changes in the activity of signaling pathways regulating cell survival and cell death [10–13,34], we decided then to study PLA/Q and PLA/PEO/Q-induced redox imbalance (Figs. 4A and S9A) and phosphorylation status of selected kinases, namely Akt and ERK1/2 in OS cells (Figs. 4B and S9B). Indeed, PLA/Q and PLA/PEO/Q promoted an elevation in superoxide levels in three OS cell lines (Fig. 4A). PLA/PEO/Q-induced oxidative stress was more pronounced than PLA/Q-induced oxidative stress in OS cells (Fig. 4A). MG-63 cells were the most susceptible to PLA/Q and PLA/PEO/Q-associated redox disequilibrium compared to other OS cells (Fig. 4A). PLA/Q and PLA/PEO/Q also promoted the activation of Akt, a survival kinase in MG-63 cells (Figs. 4B and S9B); however, this adaptive response was not able to attenuate PLA/Q and PLA/PEO/Q-induced apoptosis in these cells (Fig. 2D). This is also true in the case of PLA/PEO/Q-mediated increase in the levels of phosphorylated Akt and apoptosis induction in U-2 OS cells (Figs. 2D and 4B). In contrast, in SaOS-2 cells, quercetin-loaded fibers did not stimulate the activity of Akt (Fig. 4B). In conclusion, Akt activation in Q-loaded fiber-treated MG-63 and U-2 OS cells did not prevent against apoptotic cell death and related cytotoxicity (Figs. 2D and 4B). However, quercetin-induced apoptosis in methotrexate-resistant osteosarcoma cell line U-2 OS/MTX300 was mediated by mitochondrial dysfunction and dephosphorylation of Akt [35]. Thus, quercetin-mediated Akt inhibition/activation and related cancer cell fates may depend on experimental settings.

As Akt and pAkt (S473) are client proteins of HSP90 and quercetin can mediate its anticancer action by inhibiting the bioactivity of Akt and heat shock proteins [10,34,36–38], the levels of HSP70 and HSP90 were then analyzed upon PLA/Q and PLA/PEO/Q stimulations in OS cells (Figs. 4C and S9C). PLA/Q and PLA/PEO/Q-induced Akt activity was accompanied by elevated levels of both nuclear and cytosolic fractions of HSP70 and HSP90 upon 48 h stimulations with quercetin-loaded fibers in MG-63 cells (Fig. 4C). Similar effects, but milder, were observed after 24 h treatment with PLA/Q and PLA/PEO/Q in MG-63 cells (Fig. S9C). However, HSP-mediated protective response in PLA/Q and PLA/PEO/Q-treated MG-63 cells did not prevent or attenuate quercetin-loaded fiber-stimulated apoptosis in these cells (Fig. 2D). In SaOS-2 and U-2 OS cells, the effects of PLA/Q and PLA/PEO/Q on the levels of HSP70 and HSP90 were limited (Figs. 4C and S9C). After 48 h treatment, PLA/Q promoted the nuclear and cytosolic fractions of HSP70 in SaOS-2 cells and PLA/PEO/Q induced an increase in nuclear levels of HSP90 in U-2 OS cells (Fig. 4C). According to the literature, there are no data on quercetin-mediated effects on heat shock protein pools and related cytotoxicity in osteosarcoma. The levels of heat shock factor 1 (HSF1), HSP27 and HSP70 were compared in quercetin-treated neuroblastoma and Ewing's sarcoma cells [39]. The authors concluded that quercetin-based anti-proliferative effect was more pronounced in neuroblastoma cells with massive decrease in HSP levels compared to Ewing's sarcoma cells [39]. Moreover, HSP inhibition by quercetin potentiated sensitivity to doxorubicin [39].

3.3. The anticancer activity of quercetin-loaded fibers against breast cancer cells

The utility of quercetin-loaded fibers as anticancer universal nanoplatform was further studied using six breast cancer cell lines with different receptor and mutation status varying in drug responses, namely HER2-positive SK-BR-3 cells, ER-positive MCF-7 cells and four triple negative breast cancer (TNBC) cell lines MDA-MB-231, MDA-MB-468, Hs 578T, and BT-20 cells [30,31]. Imaging flow cytometric-based analysis revealed that PLA/Q and PLA/PEO/Q were efficiently taken up by six breast cancer cell lines (Fig. 5A). Similar to OS cells (Fig. 2C), free quercetin did not affect the metabolic activity of SK-BR-3, MCF-7 and MDA-MB-231 cells (Fig. 5B). The metabolic activity of SK-BR-3 was also not affected when these cells were stimulated with quercetin-loaded fibers (Fig. 5B). In contrast, TNBC, especially MDA-MB-468 cells, were the most sensitive to PLA/Q and PLA/PEO/Q treatments compared to other breast cancer cells, as judged by MTT results (Fig. 5B). MDA-MB-468 and SK-BR-3 cells were the most and least susceptible to PLA/Q and PLA/PEO/Q-mediated apoptotic cell death compared to other breast cancer cells, respectively (Figs. 5C and S10A). Except of Hs 578T cells, PLA/PEO/Q-induced apoptosis was more pronounced than PLA/Q-promoted apoptosis in breast cancer cells (Figs. 5C and S10A). A systemic review demonstrated that quercetin may promote apoptosis in both ER-positive and triple negative breast cancer cells that was mediated by different mechanisms, for example, oxidative stress, mitochondrial dysfunction, upregulation of proapoptotic proteins, downregulation of antiapoptotic proteins and cell cycle regulatory proteins [34]. Quercetin was also reported to reverse tamoxifen resistance in breast cancer cells by downregulation of HER2 (human epidermal growth factor receptor 2) [40]. Thus, quercetin may also limit HER2-mediated neoplastic effects in breast cancer cells [40].

We were then interested if quercetin-loaded fibers may also promote HSP-mediated protective response in breast cancer cells as observed for osteosarcoma cells (Fig. 4C). First, the basal levels of HSP70 and HSP90 were compared in six phenotypically different breast cancer cells (Fig. 6A). MDA-MB-468 and SK-BR-3 cells were characterized by the highest levels of both HSP proteins compared to other breast cancer cells in control conditions (Fig. 6A). In contrast, the control levels of HSP70 and HSP90 were the lowest in MDA-MB-231 and Hs 578T that may modulate HSP-based stress responses. Six breast cancer cell lines were then incubated with PLA/PEO/Q and the levels of HSP70 and HSP90 were monitored and compared to PLA/PEO treatment (Fig. 6B). Upon PLA/PEO/Q stimulation, HSP-mediated response was the most pronounced in TNBC cells (Fig. 6B). The highest increase in HSP70 and HSP90 levels was observed in PLA/PEO/Q-treated Hs 578T cells (Fig. 6B). In contrast, PLA/PEO/Q did not affect the levels of HSP70 and HSP90 in SK-BR-3 cells (Fig. 6B). However, HSP-based adaptive response in PLA/PEO/Q-stimulated TNBC cells did not result in the

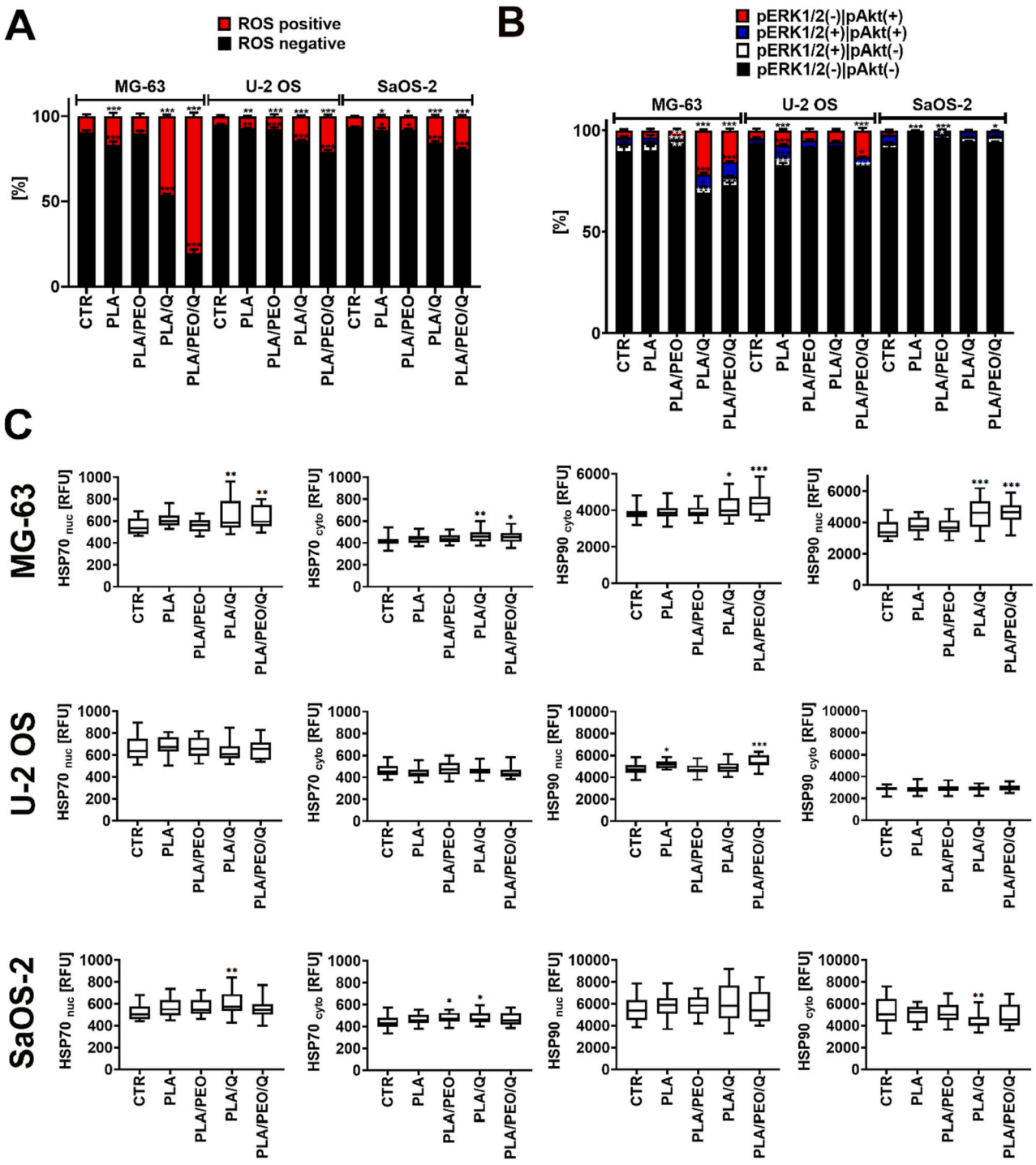

Fig. 4. Quercetin-loaded fiber-mediated oxidative stress (A), activation of Akt and ERK1/2 (B), and changes in the levels of heat shock proteins (HSP70 and HSP90) (C) in three osteosarcoma cell lines, namely MG-63, U-2 OS, and SaOS-2 cells. Cells were treated with the fibers for 48 h. (A) Oxidative stress marker was considered, namely the levels of superoxide. Superoxide levels were assessed using flow cytometry and dihydroethidium staining. Two subpopulations were revealed, namely superoxide-positive and superoxide-negative cells. (B) The activation of Akt and ERK1/2 was analyzed as phosphorylation status of Akt and ERK1/2 using flow cytometry and dedicated anti-phospho-Akt and anti-phospho-ERK1/2 antibodies. Cells with single activation (Akt activation or ERK1/2 activation) and dual activation (Akt activation and ERK1/2 activation) were distinguished. (C) Immunofluorescence-based analysis of nuclear and cytoplasmic levels of HSP70 and HSP90 was performed using imaging cytometry and dedicated anti-HSP70 and anti-HSP90 antibodies. Nuclear and cytoplasmic levels of HSP70 and HSP90 are presented as relative fluorescence units (RFU). Bars indicate SD or box and whisker plots are shown, n = 3, $^{***}p < 0.001$, $^{**}p < 0.01$, $^{*}p < 0.05$ compared to CTR untreated control (ANOVA and Dunnett's *a posteriori* test). CTR, control conditions; PLA, treatment with polylactide-based fibers; PLA/Q, treatment with polylactide-based fibers containing quercetin; PLA/PEO, treatment with polylactide and polyethylene oxide-based fibers; PLA/PEO/Q, treatment with polylactide and polyethylene oxide-based fibers containing quercetin.

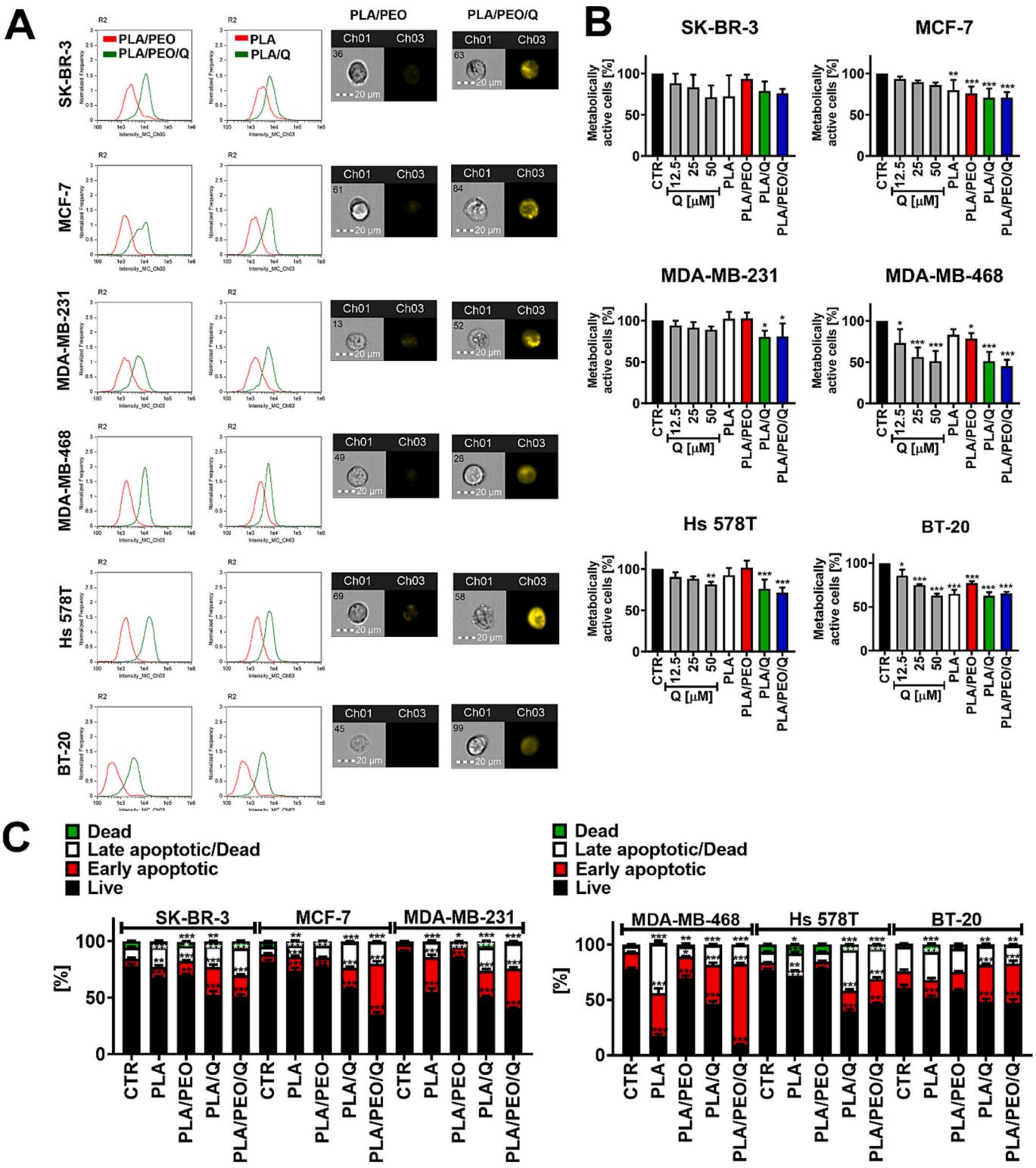

Fig. 5. PLA/Q and PLA/PEO/Q uptake (A), mediated metabolic activity (B) and apoptosis induction (C) in six breast cancer cell lines, namely SK-BR-3, MCF-7, MDA-MB-231, MDA-MB-468, Hs 578T, and BT-20 cells. Cells were treated with the fibers for 48 h. (A) Quercetin uptake was documented using imaging flow cytometry and dedicated software. Two parameters were applied, namely Normalized Frequency and Intensity_MC_Ch03. Representative microphotographs and histograms are presented. Ch01, bright field (BF); Ch03, Cyanine-3 (CY3)/orange. (B) Metabolic activity was analyzed using MTT test. Metabolic activity at untreated conditions is considered as 100 %. (D) Apoptosis was evaluated using flow cytometry and dual staining approach, namely Annexin V and 7-AAD staining. Four subpopulations were distinguished, namely live cells (dual staining-negative), early apoptotic cells (Annexin V-positive), late apoptotic cells (dual staining-positive) and necrotic cells (7-AAD-positive). Bars indicate SD, n = 3, $^{***}p < 0.001$, $^{**}p < 0.01$, $^{*}p < 0.05$ compared to CTR untreated control (ANOVA and Dunnett's *a posteriori* test). CTR, control conditions; PLA, treatment with polylactide-based fibers; PLA/Q, treatment with polylactide-based fibers containing quercetin; PLA/PEO, treatment with polylactide and polyethylene oxide-based fibers; PLA/PEO/Q, treatment with polylactide and polyethylene oxide-based fibers containing quercetin.

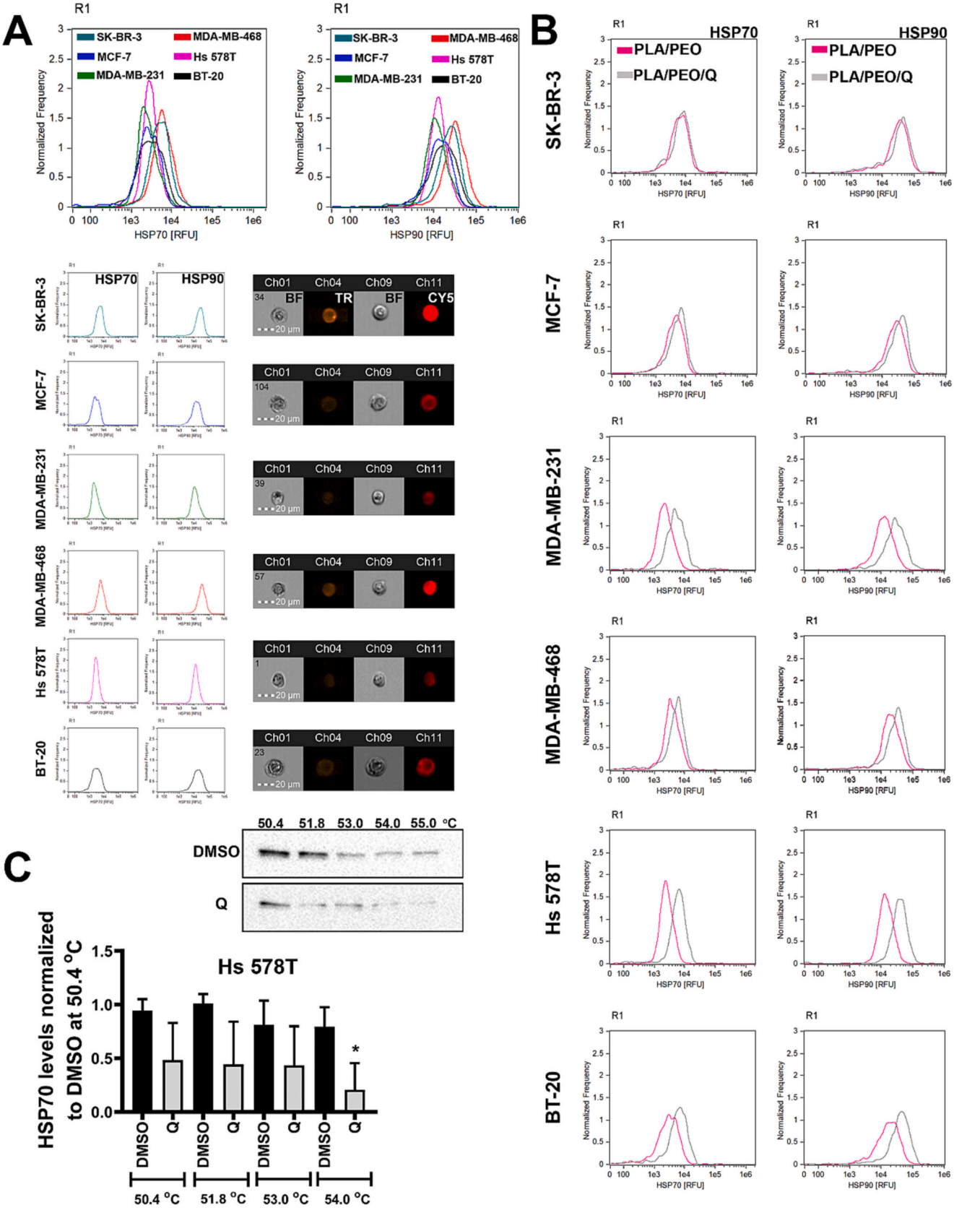

(caption on next page)

Fig. 6. Comparative analysis of HSP70 and HSP90 pools in untreated conditions (A), PLA/PEO/Q-mediated changes in HSP70 and HSP90 levels (B) and quercetin-associated stability of HSP70 (C) in six breast cancer cell lines, namely SK-BR-3, MCF-7, MDA-MB-231, MDA-MB-468, Hs 578T, and BT-20 cells. The basal levels of HSP70 and HSP90 (A) and upon stimulation with PLA/PEO/Q (B, cells were treated with the fibers for 48 h) were determined using imaging flow cytometry and dedicated anti-HSP70 and anti-HSP90 antibodies. Representative microphotographs and histograms are presented. Ch01 and Ch09, bright field (BF); Ch04, Texas Red (TR); Ch11, Cyanine-5 (CY5). (C) The interactions between quercetin and HSP70 in Hs 578T cells were studied using cellular thermal shift assay (CETSA). Upon stimulation with quercetin (Q), western blotting protocol was performed using dedicated anti-HSP70 antibody. Representative blots and densitometric analysis are shown. Data were normalized to DMSO-treated cells (DMSO was used to dissolve quercetin). A decrease in HSP70 levels indicated limited stability of HSP70 upon Q treatment. Bars indicate SD, n = 3, $*p < 0.05$ compared to DMSO-treated cells (ANOVA and Dunnett's *a posteriori* test). DMSO, treatment with dimethyl sulfoxide; Q, treatment with quercetin; PLA/PEO, treatment with polylactide and polyethylene oxide-based fibers; PLA/PEO/Q, treatment with polylactide and polyethylene oxide-based fibers containing quercetin.

suppression of apoptotic cell death (Fig. 5C). Thus, increased levels of HSP70 and HSP90 did not protect against PLA/PEO/Q-induced apoptosis in osteosarcoma (Figs. 2D and 4C) and breast cancer cells (Figs. 5C and 6B). Heat shock proteins are commonly overexpressed in breast cancer that may promote cell proliferation, apoptosis resistance, and result in poor clinical outcomes [41]. Quercetin is reported to be a heat shock protein inhibitor that induced apoptosis in breast cancer cells [38,42,43]. For example, 48 h treatment with 25 μM quercetin significantly decreased the levels of HSP27, HSP70 and HSP90 in MCF-7 and MDA-MB-231 cells [38]. As HSP-based response was the most pronounced in PLA/PEO/Q-treated Hs 578T cells (Fig. 6B), these cells were also used to study the effect of quercetin on HSP70 stabilization/degradation using cellular thermal shift assay (CETSA) (Fig. 6C). Hs 578T cells were incubated with 50 μM quercetin for 24 h that did not show any HSP70 stabilizing effect of quercetin (Fig. 6C). Instead, quercetin limited thermal stability of HSP70 as judged by decreased levels of HSP70 in quercetin-treated Hs 578T cells (Fig. 6C). Thus, the effects of PLA/PEO/Q (Fig. 6B) and free quercetin (Fig. 6C) on heat shock proteins may be diverse in Hs 578T cells.

To the best of our knowledge, there are no data on the broad-spectrum anticancer potential of PLA/Q and PLA/PEO/Q-based fibers. In general, quercetin containing electrospun fibers are studied in terms of antibacterial activity as a part of wound dressing [44]. For example, electrospun nanofiber membranes (ENM) consisting of polycaprolactone (PCL), chitosan oligosaccharides (COS) and quercetin/rutin were fabricated and tested as the potential bioactive dressing for wound healing [44]. The authors concluded that PCL-COS-quercetin membrane possessed superior performance among all nanofiber membranes [44]. Co-axial electrospinning was also used to obtain colon-specific nano-delivery system for quercetin based on chitosan nanoparticles [14,15]. However, this nano-system containing quercetin was tested against only one colon cancer cell line, namely Caco-2 cells [14,15]. Q-loaded electrospun fiber mat caused G0/G1 cell cycle arrest and promoted apoptosis in Caco-2 cells [14,15]. The authors concluded that Q-loaded electrospun fiber mat may be considered as a promising form in the oral therapy of colon disorders [14,15]. More recently, anticancer activity of electrospun cellulose acetate (CA) and polyethylene glycol (PEG) fibers containing 5 % quercetin was analyzed using a cervical cancer model *in vitro*, namely HeLa cells [16]. Q-loaded CA-PEG fibers induced apoptosis in HeLa cells as judged by AO/EtBr dual staining; however, Q-loaded electrospun fiber mat-mediated apoptosis was not documented in other cancer cells [16].

According to the literature data, there were numerous attempts to improve water solubility, chemical stability and bioavailability of quercetin by using different non-electrospun fiber-based delivery systems such as lipid-based carriers, polymer nanoparticles, inclusion complexes, micelles, and conjugates [28,45–47]. Advantages and shortcomings have been reported for each quercetin delivery system, and the use of particular DDS should be based on particular application field [28,45–47]. For example, the use of solid lipid nanoparticles (SLN) may be limited due to tendency to aggregation, recrystallization risk, and low encapsulation loading [45]. Furthermore, liposome-based systems are characterized by relatively low stability at acidic pH and high cost of raw materials, whereas conjugate-based carriers require complex preparation methods and are sensitive to pH [45]. Several disadvantages of using micelles as quercetin carriers have been also reported, namely limited solubilization capacity and high amount of surfactants or surface active agents that are needed for encapsulation [45].

3.4. Hemocompatibility of PLA/Q and PLA/PEO/Q

We have already observed that 48 h treatments with PLA/Q and PLA/PEO/Q had limited effects against normal human fibroblasts (Fig. 2C). Whole blood samples were also treated with quercetin-loaded fibers and their hemocompatibility was assessed using *in vitro* hemolysis test (Fig. S10B). Hemolytic activity of PLA/Q and PLA/PEO/Q was compared to KCl treatment (a positive control of hemolysis, 100 % of hemolysis) (Fig. S10B). 24 h stimulation with PLA/Q and PLA/PEO/Q resulted in 10 and 15 % of hemolysis compared to KCl-treated samples, respectively (Fig. S10B). However, prolonged treatment (48 h) with PLA/Q and PLA/PEO/Q caused 30 and 40 % of hemolysis compared to positive control (Fig. S10B). Thus, one can conclude that erythrocytes are relatively more sensitive to PLA/Q and PLA/PEO/Q treatments than fibroblasts (Figs. 2C and S10B).

4. Conclusions

In the present study, electrospun fibers based on polylactide, polyethylene oxide and quercetin were developed and their anticancer activity was tested for the first time using two types of cellular cancer models *in vitro*, namely osteosarcoma and breast cancer cells with different receptor status. Quercetin-loaded fibers were more effective against cancer cells compared to the action of free quercetin. Quercetin-loaded fiber-based anticancer effects were mediated by the induction of oxidative stress, cell cycle arrest and apoptosis, and inhibition of cell migration. Selective anticancer potential of quercetin-loaded fibers were documented, as judged by its limited effects against normal cells. We propose that electrospun fiber-based micro- and nano-system can be considered as a novel approach for efficient quercetin delivery to cancer cells and quercetin-mediated elimination of cancer cells by apoptotic cell death.

Funding

This work was supported by the National Science Centre (Poland) grant UMO-2021/43/B/NZ7/02129.

CRediT authorship contribution statement

A.H.: synthesis of electrospun micro- and nanofibers, conducted the experiments displayed in Table S2, conceptualization in material engineering part; **I.R.:** cell culture *in vitro*, conducted the experiments displayed in Figs. 2A, C, 3A, S8A, S10B with data analysis and data presentation; **A.L.:** conducted the experiments displayed in Figs. 2D, 3B, 4A, B, 5C, S8B, S8C, S9A, S9B, S10A, interpretation of the results, co-writing of the manuscript; **T.W.:** conducted the experiments displayed in Figs. 1E, G, S2D, S3D, S4D, S2E, S3E, S4E, S6 with data analysis and data presentation; **A. B-K.:** conducted the experiments displayed in Figs. 1H, I, J, K, L, S2F, S3F, S4F, Table S1 with data analysis and data presentation; **R.W-N.:** conducted the experiments displayed in Figs. 1M,

S5 and S7 with data analysis and data presentation; **G.B.:** conducted the experiments displayed in Figs. 2E, 5B with data analysis and data presentation, cell culture *in vitro*; **A.D.:** conducted the experiments displayed in Fig. 6C with data analysis and data presentation; **J.H.:** conducted the experiments displayed in Figs. 1C, S2C, S3C, S4C with data analysis and data presentation; **D. L-M.:** conducted the experiments displayed in Fig. 1F; **W.L.:** conducted the experiments displayed in Fig. 1D; **A.M.:** conducted the experiments displayed in Fig. 3C; **P.K.:** conducted the experiments displayed in Fig. S1 with data analysis and data presentation; **M.C.:** interpretation of the results of material part; **M. K-B.:** interpretation of the results of material part; **A.K-B:** conducted the experiments displayed in Figs. 1A, B, S2A, S2B, S3A, S3B, S4A, S4B with data analysis and data presentation, interpretation of the results of material part and supervision of material engineering part; **M.W.:** conducted the experiments displayed in Figs. 2B, 4C, 5A, 6A, B, S9C, co-writing of the manuscript, conceptualization in biological part, interpretation of *in vitro* cell model results and supervision of cell biology part.

Declaration of competing interest

The authors declare the following financial interests/personal relationships which may be considered as potential competing interests: Maciej Wnuk reports financial support was provided by National Science Centre Poland.

Data availability

The data presented in this study are available in the supplementary material.

Acknowledgement

We would like to thank two anonymous reviewers for their feedback, which helped us to improve the manuscript and focus on our further work.

Appendix A. Supplementary data

Supplementary data to this article can be found online at https://doi.org/10.1016/j.bioadv.2023.213582.

References

[1] O.S. Fenton, K.N. Olafson, P.S. Pillai, M.J. Mitchell, R. Langer, Advances in biomaterials for drug delivery, Adv. Mater. 30 (2018) 1705328, https://doi.org/10.1002/adma.201705328.
[2] X. Feng, J. Li, X. Zhang, T. Liu, J. Ding, X. Chen, Electrospun polymer micro/nanofibers as pharmaceutical repositories for healthcare, J. Control. Release 302 (2019) 19–41, https://doi.org/10.1016/j.jconrel.2019.03.020.
[3] A. Luraghi, F. Peri, L. Moroni, Electrospinning for drug delivery applications: a review, J. Control. Release 334 (2021) 463–484, https://doi.org/10.1016/j.jconrel.2021.03.033.
[4] A. Khalf, S.V. Madihally, Recent advances in multiaxial electrospinning for drug delivery, Eur. J. Pharm. Biopharm. 112 (2017) 1–17, https://doi.org/10.1016/j.ejpb.2016.11.010.
[5] H. Luo, T. Jie, L. Zheng, C. Huang, G. Chen, W. Cui, Electrospun nanofibers for cancer therapy, in: F. Fontana, H.A. Santos (Eds.), Bio-Nanomedicine Cancer Ther, Springer International Publishing, Cham, 2021, pp. 163–190, https://doi.org/10.1007/978-3-030-58174-9_8.
[6] B. Abadi, N. Goshtasbi, S. Bolourian, J. Tahsili, M. Adeli-Sardou, H. Forootanfar, Electrospun hybrid nanofibers: fabrication, characterization, and biomedical applications, Front. Bioeng. Biotechnol. 10 (2022), 986975, https://doi.org/10.3389/fbioe.2022.986975.
[7] B. Salehi, L. Machin, L. Monzote, J. Sharifi-Rad, S.M. Ezzat, M.A. Salem, R. M. Merghany, N.M. El Mahdy, C.S. Kılıç, O. Sytar, M. Sharifi-Rad, F. Sharopov, N. Martins, M. Martorell, W.C. Cho, Therapeutic potential of quercetin: new insights and perspectives for human health, ACS Omega. 5 (2020) 11849–11872, https://doi.org/10.1021/acsomega.0c01818.
[8] M. Russo, C. Spagnuolo, I. Tedesco, S. Bilotto, G.L. Russo, The flavonoid quercetin in disease prevention and therapy: facts and fancies, Biochem. Pharmacol. 83 (2012) 6–15, https://doi.org/10.1016/j.bcp.2011.08.010.
[9] I. Shabir, V. Kumar Pandey, R. Shams, A.H. Dar, K.K. Dash, S.A. Khan, I. Bashir, G. Jeevarathinam, A.V. Rusu, T. Esatbeyoglu, R. Pandiselvam, Promising bioactive properties of quercetin for potential food applications and health benefits: a review, Front. Nutr. 9 (2022), 999752, https://doi.org/10.3389/fnut.2022.999752.
[10] M. Ezzati, B. Yousefi, K. Velaei, A. Safa, A review on anti-cancer properties of quercetin in breast cancer, Life Sci. 248 (2020), 117463, https://doi.org/10.1016/j.lfs.2020.117463.
[11] P. Maleki Dana, F. Sadoughi, Z. Asemi, B. Yousefi, Anti-cancer properties of quercetin in osteosarcoma, Cancer Cell Int. 21 (2021) 349, https://doi.org/10.1186/s12935-021-02067-8.
[12] A. Maugeri, A. Calderaro, G.T. Patanè, M. Navarra, D. Barreca, S. Cirmi, M. R. Felice, Targets involved in the anti-cancer activity of quercetin in breast, colorectal and liver neoplasms, Int. J. Mol. Sci. 24 (2023) 2952, https://doi.org/10.3390/ijms24032952.
[13] N. Kasiri, M. Rahmati, L. Ahmadi, N. Eskandari, H. Motedayyen, Therapeutic potential of quercetin on human breast cancer in different dimensions, Inflammopharmacology. 28 (2020) 39–62, https://doi.org/10.1007/s10787-019-00660-y.
[14] P. Wen, T.-G. Hu, L. Li, M.-H. Zong, H. Wu, A colon-specific delivery system for quercetin with enhanced cancer prevention based on co-axial electrospinning, Food Funct. 9 (2018) 5999–6009, https://doi.org/10.1039/C8FO01216D.
[15] P. Wen, M.-H. Zong, T.-G. Hu, L. Li, H. Wu, Preparation and characterization of electrospun colon-specific delivery system for quercetin and its antiproliferative effect on cancer cells, J. Agric. Food Chem. 66 (2018) 11550–11559, https://doi.org/10.1021/acs.jafc.8b02614.
[16] N. Stoyanova, M. Spasova, N. Manolova, I. Rashkov, A. Georgieva, R. Toshkova, Quercetin- and rutin-containing electrospun cellulose acetate and polyethylene glycol fibers with antioxidant and anticancer properties, Polymers. 14 (2022) 5380, https://doi.org/10.3390/polym14245380.
[17] A. Lewinska, J. Adamczyk-Grochala, E. Kwasniewicz, A. Deregowska, E. Semik, T. Zabek, M. Wnuk, Reduced levels of methyltransferase DNMT2 sensitize human fibroblasts to oxidative stress and DNA damage that is accompanied by changes in proliferation-related miRNA expression, Redox Biol. 14 (2018) 20–34, https://doi.org/10.1016/j.redox.2017.08.012.
[18] A. Lewinska, J. Adamczyk-Grochala, D. Bloniarz, J. Olszowka, M. Kulpa-Greszta, G. Litwinienko, A. Tomaszewska, M. Wnuk, R. Pazik, AMPK-mediated senolytic and senostatic activity of quercetin surface functionalized Fe_3O_4 nanoparticles during oxidant-induced senescence in human fibroblasts, Redox Biol. 28 (2020), 101337, https://doi.org/10.1016/j.redox.2019.101337.
[19] C.R. Justus, N. Leffler, M. Ruiz-Echevarria, L.V. Yang, *In vitro* cell migration and invasion assays, J. Vis. Exp. (2014), 51046, https://doi.org/10.3791/51046.
[20] R. Jafari, H. Almqvist, H. Axelsson, M. Ignatushchenko, T. Lundbäck, P. Nordlund, D.M. Molina, The cellular thermal shift assay for evaluating drug target interactions in cells, Nat. Protoc. 9 (2014) 2100–2122, https://doi.org/10.1038/nprot.2014.138.
[21] K. Wróbel, A. Deręgowska, G. Betlej, M. Walczak, M. Wnuk, A. Lewińska, S. Wołowiec, Cytarabine and dexamethasone-PAMAM dendrimer di-conjugate sensitizes human acute myeloid leukemia cells to apoptotic cell death, J. Drug Deliv. Sci. Technol. 81 (2023), 104242, https://doi.org/10.1016/j.jddst.2023.104242.
[22] D.L. Puhl, J.L. Funnell, D.W. Nelson, M.K. Gottipati, R.J. Gilbert, Electrospun fiber scaffolds for engineering glial cell behavior to promote neural regeneration, Bioengineering. 8 (2020) 4, https://doi.org/10.3390/bioengineering8010004.
[23] M.K. Haidar, S.S. Timur, G.M. Demirbolat, E. Nemutlu, R.N. Gürsoy, K. Ulubayram, L. Öner, H. Eroğlu, Electrospun nanofibers for dual and local delivery of neuroprotective drugs, Fibers Polym. 22 (2021) 334–344, https://doi.org/10.1007/s12221-021-0228-2.
[24] X. Li, Y. He, J. Hou, G. Yang, S. Zhou, A time-programmed release of dual drugs from an implantable trilayer structured fiber device for synergistic treatment of breast cancer, Small. 16 (2020) 1902262, https://doi.org/10.1002/smll.201902262.
[25] I.C.C.M. Porto, T.G. Nascimento, J.M.S. Oliveira, P.H. Freitas, A. Haimeur, R. França, Use of polyphenols as a strategy to prevent bond degradation in the dentin-resin interface, Eur. J. Oral Sci. 126 (2018) 146–158, https://doi.org/10.1111/eos.12403.
[26] B. Pawlikowska-Pawlęga, H. Dziubińska, E. Król, K. Trębacz, A. Jarosz-Wilkołazka, R. Paduch, A. Gawron, W.I. Gruszecki, Characteristics of quercetin interactions with liposomal and vacuolar membranes, Biochim. Biophys. Acta BBA - Biomembr. 2014 (1838) 254–265, https://doi.org/10.1016/j.bbamem.2013.08.014.
[27] R.G.R. Pinheiro, M. Pinheiro, A.R. Neves, Nanotechnology innovations to enhance the therapeutic efficacy of quercetin, Nanomaterials. 11 (2021) 2658, https://doi.org/10.3390/nano11102658.
[28] X. Zang, M. Cheng, X. Zhang, X. Chen, Quercetin nanoformulations: a promising strategy for tumor therapy, Food Funct. 12 (2021) 6664–6681, https://doi.org/10.1039/D1FO00851J.
[29] G. Betlej, T. Ząbek, A. Lewińska, D. Błoniarz, I. Rzeszutek, M. Wnuk, RNA 5-methylcytosine status is associated with DNMT2/TRDMT1 nuclear localization in osteosarcoma cell lines, J. Bone Oncol. 36 (2022), 100448, https://doi.org/10.1016/j.jbo.2022.100448.
[30] D.L. Holliday, V. Speirs, Choosing the right cell line for breast cancer research, Breast Cancer Res. 13 (2011) 215, https://doi.org/10.1186/bcr2889.
[31] X. Dai, H. Cheng, Z. Bai, J. Li, Breast cancer cell line classification and its relevance with breast tumor subtyping, J. Cancer 8 (2017) 3131–3141, https://doi.org/10.7150/jca.18457.

[32] D. Catanzaro, E. Ragazzi, C. Vianello, L. Caparrotta, M. Montopoli, Effect of quercetin on cell cycle and cyclin expression in ovarian carcinoma and osteosarcoma cell lines, Nat. Prod. Commun. 10 (2015) 1365–1368.
[33] J.-A. Choi, J.-Y. Kim, J.-Y. Lee, C.-M. Kang, H.-J. Kwon, Y.-D. Yoo, T.-W. Kim, Y.-S. Lee, S.-J. Lee, Induction of cell cycle arrest and apoptosis in human breast cancer cells by quercetin, Int. J. Oncol. (2001), https://doi.org/10.3892/ijo.19.4.837.
[34] R. Molani Gol, S. Kheirouri, The effects of quercetin on the apoptosis of human breast cancer cell lines MCF-7 and MDA-MB-231: a systematic review, Nutr. Cancer 74 (2022) 405–422, https://doi.org/10.1080/01635581.2021.1897631.
[35] J. Shen, Quercetin induces apoptosis in the methotrexate-resistant osteosarcoma cell line U2-OS/MTX300 via mitochondrial dysfunction and dephosphorylation of Akt, Oncol. Rep. (2011), https://doi.org/10.3892/or.2011.1328.
[36] S. Sato, N. Fujita, T. Tsuruo, Modulation of Akt kinase activity by binding to Hsp90, Proc. Natl. Acad. Sci. 97 (2000) 10832–10837, https://doi.org/10.1073/pnas.170276797.
[37] R. Aalinkeel, B. Bindukumar, J.L. Reynolds, D.E. Sykes, S.D. Mahajan, K.C. Chadha, S.A. Schwartz, The dietary bioflavonoid, quercetin, selectively induces apoptosis of prostate cancer cells by down-regulating the expression of heat shock protein 90, Prostate 68 (2008) 1773–1789, https://doi.org/10.1002/pros.20845.
[38] E. Kıyga, A. Şengelen, Z. Adıgüzel, E. Önay Uçar, Investigation of the role of quercetin as a heat shock protein inhibitor on apoptosis in human breast cancer cells, Mol. Biol. Rep. 47 (2020) 4957–4967, https://doi.org/10.1007/s11033-020-05641-x.
[39] C. Zanini, G. Giribaldi, G. Mandili, F. Carta, N. Crescenzio, B. Bisaro, A. Doria, L. Foglia, L.C. di Montezemolo, F. Timeus, F. Turrini, Inhibition of heat shock proteins (HSP) expression by quercetin and differential doxorubicin sensitization in neuroblastoma and Ewing's sarcoma cell lines, J. Neurochem. 103 (2007) 1344–1354, https://doi.org/10.1111/j.1471-4159.2007.04835.x.
[40] H. Wang, L. Tao, K. Qi, H. Zhang, D. Feng, W. Wei, H. Kong, T. Chen, Q. Lin, Quercetin reverses tamoxifen resistance in breast cancer cells, J. Buon Off. J. Balk. Union Oncol. 20 (2015) 707–713.
[41] L.S. Kim, J.H. Kim, Heat shock protein as molecular targets for breast cancer therapeutics, J. Breast Cancer 14 (2011) 167, https://doi.org/10.4048/jbc.2011.14.3.167.
[42] R.K. Hansen, S. Oesterreich, P. Lemieux, K.D. Sarge, S.A.W. Fuqua, Quercetin inhibits heat shock protein induction but not heat shock factor DNA-binding in human breast carcinoma cells, Biochem. Biophys. Res. Commun. 239 (1997) 851–856, https://doi.org/10.1006/bbrc.1997.7572.
[43] W. Yang, M. Cui, J. Lee, W. Gong, S. Wang, J. Fu, G. Wu, K. Yan, Heat shock protein inhibitor, quercetin, as a novel adjuvant agent to improve radiofrequency ablation-induced tumor destruction and its molecular mechanism, Chin. J. Cancer Res. Chung-Kuo Yen Cheng Yen Chiu. 28 (2016) 19–28, https://doi.org/10.3978/j.issn.1000-9604.2016.02.06.
[44] L. Zhou, L. Cai, H. Ruan, L. Zhang, J. Wang, H. Jiang, Y. Wu, S. Feng, J. Chen, Electrospun chitosan oligosaccharide/polycaprolactone nanofibers loaded with wound-healing compounds of Rutin and Quercetin as antibacterial dressings, Int. J. Biol. Macromol. 183 (2021) 1145–1154, https://doi.org/10.1016/j.ijbiomac.2021.05.031.
[45] W. Wang, C. Sun, L. Mao, P. Ma, F. Liu, J. Yang, Y. Gao, The biological activities, chemical stability, metabolism and delivery systems of quercetin: a review, Trends Food Sci. Technol. 56 (2016) 21–38, https://doi.org/10.1016/j.tifs.2016.07.004.
[46] K. Wadhwa, V. Kadian, V. Puri, B.Y. Bhardwaj, A. Sharma, R. Pahwa, R. Rao, M. Gupta, I. Singh, New insights into quercetin nanoformulations for topical delivery, Phytomedicine Plus. 2 (2022), 100257, https://doi.org/10.1016/j.phyplu.2022.100257.
[47] E.-M. Tomou, P. Papakyriakopoulou, E.-M. Saitani, G. Valsami, N. Pippa, H. Skaltsa, Recent advances in nanoformulations for quercetin delivery, Pharmaceutics. 15 (2023) 1656, https://doi.org/10.3390/pharmaceutics15061656.